BIFURCATION ANALYSIS OF A MODEL OF THE FROG EGG CELL CYCLE

Mark T. Borisuk

Dissertation submitted to the Faculty of the

Virginia Polytechnic Institute and State University

in partial fulfillment of the requirements for the degree of

Doctor of Philosophy
in
Mathematics

John J. Tyson, Co-Chair
Terry L. Herdman, Co-Chair
John A. Burns
Eugene M. Cliff
Kenneth P. Hannsgen

May, 1997
Blacksburg, Virginia

Bifurcation Analysis of a Model of the Frog Egg Cell Cycle

by
Mark T. Borisuk
Committee Co-Chairmen: John J. Tyson, Terry L. Herdman
Departments of Biology and Mathematics

ABSTRACT

Fertilized frog eggs (and cell-free extracts) undergo periodic oscillations in the activity of "M-phase promoting factor" (MPF), the crucial triggering enzyme for mitosis (nuclear division) and cell division. MPF activity is regulated by a complex network of biochemical reactions. Novak and Tyson, and their collaborators, have been studying the qualitative and quantitative properties of a large system of nonlinear ordinary differential equations that describe the molecular details of this system as currently known. Important clues to the behavior of the model are provided by bifurcation theory, especially characterization of the codimension-1 and -2 bifurcation sets of the differential equations. To illustrate this method, I have been studying a system of 9 ordinary differentail equations that describe the frog egg cell cycle with some fidelity. I will describe the bifurcation diagram of this system in a parameter space spanned by the rate constants for cyclin synthesis and cyclin degradation. My results suggest either that the cell cycle control system should show dynamical behavior considerably more complex than the limit cycles and steady states reported so far, or that the biochemical rate constants of the system are constrained to avoid regions of parameter space where complex bifurcation points unfold.

Acknowledgement

I am sincerely grateful to my co-chairman, Dr. John J. Tyson, for his willingness to work with me and his patience and encouragement throughout my research. His enthusiasm in this area of research has not only been contagious but has made my time as a graduate student very enjoyable. I am also grateful to my co-chairman, Dr. Terry L. Herdman for his encouragement to me since the beginning of my time in graduate school. He has helped me to learn, understand, and appreciate mathematics and its applications, and has given me much sound advice thoughout this entire process. I would like to thank the other members of my committee: Dr. Eugene M. Cliff for his kindness and patience in answering a variety of computer related questions, Dr. Kenneth P. Hannsgen for his interest and encouragement in this project, as well as my development as a teacher, and Dr. John A. Burns for enabling me to succeed in my first prelim course–Calculus of Variation.

I would like to acknowledge and thank the Interdisciplinary Center for Applied Mathematics and the Air Force Office of Scientific Research for their support under grant F49620-93-1-0280.

I am grateful to Dr. John Guckenheimer for his consultation on this work. I would like to thank Dr. John Burkhardt for his help with the different software packages used for this research. I am also greatly indebted to the authors of AUTO.

I would like to thank my parents, Benjamin and Elizabeth Borisuk, for their continued encouragment and love during this project and throughout my life.

I am especially grateful to my wife Charity for her help, encouragement, and support. I thank her for typing the majority of this work and for doing the most important job of being a mother to Grace, Elizabeth, and Anna who are the joy of our lives.

Most importantly, I acknowledge my Lord and Savior, Jesus Christ through Whom I "live and move and exist" (Acts 17:28). I have spent a decade entrenched in the halls of academia searching for knowledge and have been truly blessed by the revelation that "The fear of the Lord is the beginning of knowledge" (Proverbs 1:7). I trust my life has and will continue to reflect the humility and love towards my fellow man that Christ demonstrated while he was on this earth.

I dedicate this dissertation to my precious wife Charity.

Preface

The interdisciplinary nature of this research has made a fairly detailed introduction to both the biology and the mathematics necessary. My goal has been to give enough information so that this document is, for the most part, self contained for readers from either field. I am sure I have not acomplished this completely. However, I hope that with a careful reading, the reader will come away with a better understanding of the cell cycle and bifurcation theory, and a better appreciation for the complexity of biological systems and the usefulness of mathematics in dealing with this complexity.

Chapter 1 is a general introduction to the cell cycle and how it is regulated and controlled. In Chapter 2, we look in greater depth at the biochemical details and information about M-phase control that has been found through the study of frog eggs. The chapter ends with a summary of the derivation of a mathematical model. Chapter 3 begins with an introduction to the theory of systems of nonlinear differential equations. We also introduce bifurcation theory and chapter ends with a detailed look at each of the bifurcations that are found in the Xenopus model. Figures generated from my research are included in Chapter 3 as examples of the different bifurcations. Results from my analysis of these equations is discussed in Chapter 4 and their relation to the embryonic cell cycle in frog eggs is discussed in the final chapter.

I have used the continuation and bifurcation software AUTO [21], extensively for this research. I have also used DSTool (Dynamical System Tool) [22] and HOMCONT [23].

Contents

List of Figures

Chapter 1

The Cell Cycle

1.1 The Physiology of the Cell Cycle

"Without understanding how the cell cycle works, we cannot understand how the fusion of two cells, an egg and a sperm, and the subsequent divisions of the fertilized egg produce an adult human composed of about 10^{13} cells. Without knowing the checks and balances that normally insure orderly cell division, we cannot devise effective strategies to combat the uncontrolled cell division of the cancers that will kill one in six of us" [1].

That all cells are derived from previously existing cells by the process of cell division is a fundamental tenet of cell biology. The adult human is producing millions of new cells each second to replace cells lost by the normal wear and tear of life. Simply stated, cells reproduce by duplicating their contents and then dividing in two. There are basically four tasks that a cell must complete during the cell cycle: double its mass, replicate its DNA, segregate its chromosomes into two identical sets, and divide into two daughter cells.

Several distinctions can be made between different types of cells. First of all, cells whose DNA is enclosed in a nucleus are called eukaryotic cells, whereas prokaryotic cells, like bacteria, have no membrane separating nucleus from cytoplasm. Some cells live as unicellular organisms with only a small amount of interaction with each other (e.g. yeast cells, most prokaryotes), whereas multicellular organisms are comprised of groups of cells that interact and co-operate with each other. In complex organisms, different types of cells are specialized for different functions. It is estimated that mammals have as many as 200 different cell types. "Despite their complicated patterns of interdependence, cells in multicellular

organisms are distinct entities with considerable autonomy. They are responsible for their own maintenance, and in principle, they can grow and divide independently of their neighbors. In practice, however, organisms regulate cell growth and division according to a set of strict 'social' rules. Violation of these rules leads to cancer and ultimately the death of the organism" [1].

Despite their complexity, most cells are very small. An average bacterial cell is less than 2 microns long (1 micron = 10^{-6} m) and an average human cell is less than 20 microns in diameter. Nevertheless there are some exceptions. As we will see, frog eggs can be as large as 1 mm in diameter or large enough to contain 10^9 bacteria. Even though different cell types within an organism have varying sizes, cell size is fairly constant within the same cell type. What governs the size of cells is not completely understood at this time.

The duration of the cell cycle is very different in various types of cells. The shortest known cycle is in early embryogenesis of the fruit fly egg, when each cell divides every 8 minutes. On the other hand, mammalian liver cells may divide only once a year. Some cells, such as neurons, have left the cell cycle and never divide again. A more typical example would be intestinal crypt cells which divide about once per day to replenish the lining of the digestive tract.

The cell cycle (Fig. 1.1) is divided into two main phases: DNA synthesis (S phase) and mitosis (M phase). These two phases are temporally distinct and separated by two "gaps", G1 and G2. In rapidly dividing human cells, G1 typically lasts about 12 hours, S phase 6 hours, G2 6 hours, and mitosis lasts about 30 minutes. Overall cell growth occurs continually throughout the cycle, although often there is a pause in growth while the nucleus and cytoplasm are dividing. During S phase, the chromosomes which contain the DNA are replicated, producing an exact copy of the DNA. G2 is the gap between S phase and M phase, and the DNA content of a G1 cell is one-half that of a cell in G2 or M phase. G1 is the gap after M phase and before the next S phase. The most dramatic part of the cell cycle is M phase. During mitosis, the chromosomes become aligned on the mitotic spindle, ready for segregation. The nuclear envelope surrounding the replicated chromosomes breaks down, and mitosis ends with spatial separation of the two DNA copies, reconstruction of two nuclei, and division into two daughter cells. Cell division can occur in several ways. Animal cells pinch in half by a process called cytokinesis. Plants and other organisms that have rigid cell walls produce a new cell wall in the center of the cell.

A cell needs between 2000 and 5000 different enzymes and structural proteins to grow and divide [1]. There are many different types of proteins within a cell, each designed for a specific role. "Important classes include the enzymes that produce the building blocks for the synthesis of DNA, RNA, and proteins and the enzymes that use these building blocks to replicate DNA, transcribe DNA into RNA, and translate mRNA into protein" [1].

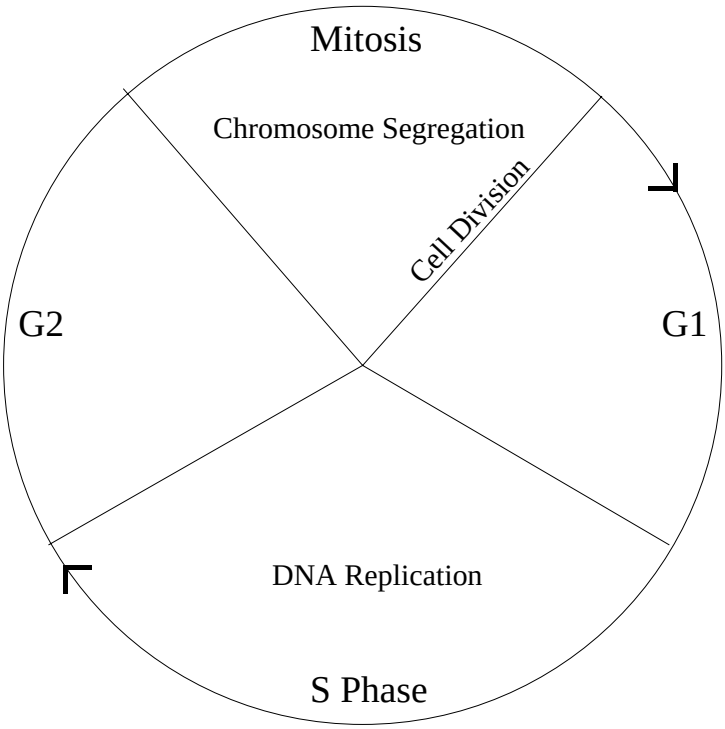

Figure 1.1: The Cell Cycle.

Protein phosphorylation and dephosphorylation is a common way to regulate the activity of proteins during the cell cycle. Enzymes that regulate protein phosphorylation are like keys or molecular switches that turn on and off the target protein. Protein kinases add phosphate groups to target proteins, whereas protein phosphatases remove the phosphate groups. The behavior of the target protein can be dramatically altered by the addition or removal of phosphate groups. Another important family of proteins involved in regulation of the cell cycle is the cyclins. Cyclins are specialized proteins that bind to cyclin-dependent protein kinases (Cdk) and control their ability to phosphorylate appropriate target proteins. The cyclic assembly, activation, and disassembly of cyclin-Cdk complexes are the pivotal events driving the cell cycle [2]. Cyclins (as indicated by the name) undergo a cycle of synthesis and degradation during each cell cycle. There are basically two main classes of cyclins. The ones we will be studying in the frog egg model are mitotic cyclins which bind to Cdk molecules during G2 and are required for entry into mitosis. Also, there are G1 cyclins which bind to Cdk molecules during G1 and are required for entry into S phase. Alberts et al. [2] describes the events that drive the cell into and out of mitosis as follows: "Mitotic cyclin accumulates gradually during G2 and binds to Cdk (Cdc2) to form a complex known as M-phase-promoting factor (MPF). This complex is at first inactive, but through the action of other enzymes that phosphorylate and dephosphorylate it, it is converted to an active form. The ultimate activation of MPF is almost explosive. This is believed to be due to a positive feedback mechanism whereby active MPF increases the activity of the enzymes that activate MPF: thus the concentration of active MPF builds up at an accelerating pace until a critical flashpoint is reached, whereupon a flood of active MPF triggers the downstream events that propel the cell into mitosis. MPF is inactivated equally suddenly by the degradation of mitotic cyclin at the metaphase-anaphase boundary, enabling the cell to exit from mitosis."

Chapter 2

Xenopus Model

In this chapter we will examine the biology and chemistry of the cell cycle in frog eggs (Sec 2.1) and then put everything together (Sec 2.2) into a biochemical mechanism of the M-phase control system. In Sections 2.3 and 2.4 we summarize the derivation of a mathematical model based on the molecular mechanism. Most of this chapter is based on a paper, *Numerical Analysis of a Comprehensive Model of M-Phase Control in Xenopus Oocyte Extracts and Intact Embryos*, by Novak and Tyson [3].

2.1 Description and Relation to Mitosis

The study of eggs from *Xenopus laevis* (a species of frog found in Africa) has been extremely beneficial in gaining insights into the cell cycle. This is true for several reasons. First, the frog egg is very large (1mm) in comparison to most cells and therefore simpler to experiment on.

Second, because the cells of a newly fertilized egg pass through the cell cycle in synchrony, it is easier to measure the activity of proteins that fluctuate in a cell-cycle dependent manner. After the egg is fertilized, the first cell cycle lasts 75 minutes. This is then followed by 11 sychronous cell divisions each lasting approximately 30 minutes. Since the frog egg has already inherited nutrients from the mother, G1 and G2 phases are largely compressed. Therefore there are multiple cells (during the last division about 2048 cells) entering mitosis at exactly the same time, making it easier to see the activity of certain proteins.

Third, cell free extracts prepared from frog eggs exhibit many of the same properties as the intact egg and are much easier to manipulate. Finally, the proteins found to induce mitosis in frog eggs are also active in other eukaryotic cells (including human cells).

"They occur without growth and at extraordinary speed and lack most of the usual checks and controls. These early embryonic cell cycles reveal the workings of the cell-cycle control system stripped down and simplified to the bare minimum needed to achieve the most fundamental requirement–the duplication of the genome and its segregation into two daughter cells. Although these cell cycles are exceptional, they illuminate the mechanisms of the division cycle in all eukaryotic cells" [2].

Mitosis Promoting Factor and the Discovery of Cyclin

A mitosis-inducing protein was discovered, called MPF (mitosis promotion factor), which is high at every mitosis but low during every interphase. It was also found that periodic MPF activation is a purely cytoplasmic process. That is to say, MPF activity is generated by a cytoplasmic oscillator that operates even in the absence of the nucleus (e.g. DNA synthesis). However, MPF activity was blocked by inhibition of protein synthesis.

It was observed that during the egg cell cycle most proteins increased monotonically after fertilization except for one distinctive protein. Cyclin, as it was later named, increased during interphase and then declined abruptly during mitosis, in a periodic or cyclic fashion. When MPF was finally purified, it was found to consist of two different subunits: a cyclin-dependent protein kinase called Cdc2 and a mitotic cyclin. This observation suggests a simple model of the embryonic cell cycle: "... the accumulation of cyclin during interphase activates MPF, active MPF induces the destruction of cyclin, and the destruction of cyclin leads to the inactivation of MPF. In this model the cell cycle engine flip-flops periodically between mitosis and interphase" [1].

As will be seen, this model does not tell the whole story. For one thing, the activation of MPF is an autocatalytic process. In other words, MPF induces its own activation. Furthermore, the activation of MPF is not governed exclusively by cyclin synthesis but also depends on regulation of the Cdc2 subunit by other proteins. There are three important phosphorylation sites that regulate the activity of MPF: an activatory phosphorylation site at threonine-161 (Thr161) and two inhibitory phosphorylation sites at threonine-14 (Thr14) and tyrosine-15 (Tyr15). In Xenopus the two inhibitory sites are dephosphorylated simultaneously, so it is sufficient to keep track only of the phosphorylation state of Tyr15. Therefore, as we will see in Fig. 2.1, this makes for four different phosphorylation states of the Cdc2-cyclin dimer.

Previously, it was mentioned that cyclic activation of MPF is not dependent on DNA synthesis, at least for the first few embryonic cycles. This is because the amount of DNA and therefore DNA dependent signals are too weak to be received by the cytoplasmic control system. However, over the first 12 division cycles the ratio of DNA to cytoplasm increases by a factor of 4000. Therefore, in the later cycles some of the feedback controls of the standard cell cycle begin to operate. Finally, MPF causes its own destruction by indirectly stimulating the ubiquitin-conjugation pathway which labels cyclin for destruction, thereby creating a negative feedback loop. Both the positive and negative feedback loop of MPF operate with significant time delays that seem to have important physiological consequences.

2.2 Biochemical Model

Fig. 2.1 is a biochemical mechanism of mitotic control. Cyclin is represented by an oval and Cdc2 is represented by a rectangle. The two arms on the rectangle are representative of the principal phosphorylation sites of Cdc2: tyrosine-15 (Y) on the left and theonine-161 (T) on the right. Wee1 and Cdc25, named after the genes *wee1* and *cdc25* in fission yeast, are the kinase and phosphatase that regulate the phosphorylation of Tyr15. As can be seen by the direction of the arrows, Tyr15 is phosphorylated by Wee1 and dephosphorylated by Cdc25. Likewise, Thr161 is phosphorylated by an enzyme called CAK (Cdc2 activating kinase) and dephosphorylated by an unknown phosphatase (PP?).

Part *A* of Fig. 2.1 shows the four phosphorylation states of MPF and how they are formed. In step 1 cyclin subunits are synthesized from amino acids by the cell. Step 2 indicates degradation of free cyclin by a ubiquitination pathway. (The degradation of dimers will appear in part *C*). Cyclin subunits bind with free Cdc2 monomers in step 3 to form Cdc2-cyclin dimers. Because of the action of the two kinase-phosphatase pairs, Wee1/Cdc25 and CAK/PP?, the dimer can exist in four different phosphorylation states. Therefore Fig. 2.1 part *A* is referred to as the dimer box. The dimer in the upper right corner of the box is active MPF. When the amount of MPF reaches a certain level, it initiates mitosis by phosphorylating other proteins.

Part *B* of Fig. 2.1 shows that active MPF stimulates its own production from the tyrosine-phosphorylated dimers by inhibiting Wee1 and activating Cdc25. The signals from active MPF to Wee1 and Cdc25 generate an autocatalytic instability. Also, unreplicated DNA sends an 'external' signal to Wee1 and Cdc25. These signals play a role in the efficacy of the positive feedback loop. The letters a, b, e, and f are used to label the rate constants for these reactions [3].

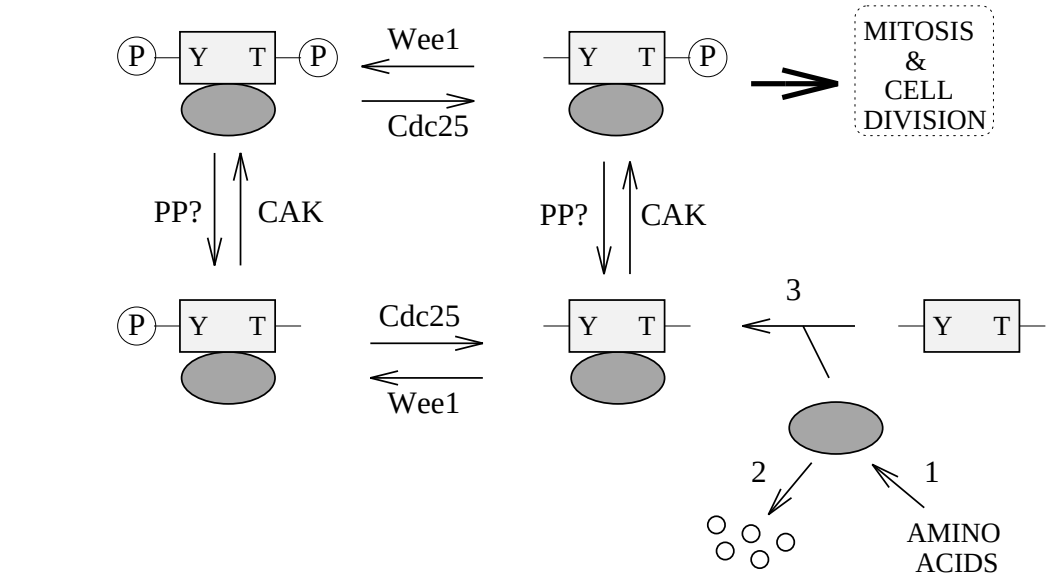

A. The Phosphorylation States of MPF

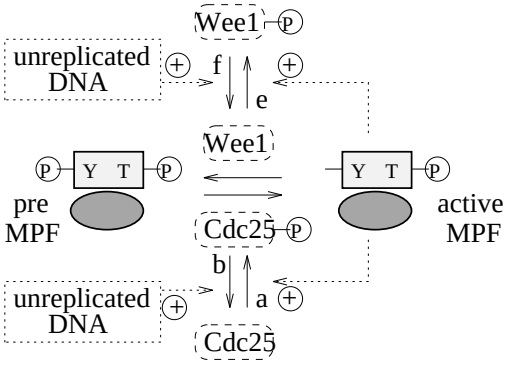

B. Positive Feedback Loops

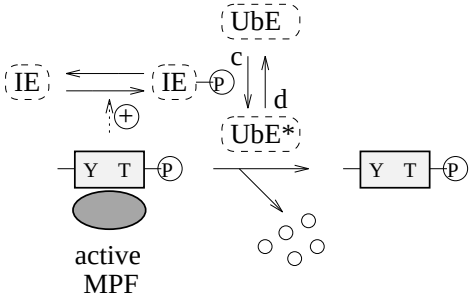

C. Negative Feedback Loop

Figure 2.1: The M-phase Control System (Novak and Tyson [3, Fig.1]).

Part C of Fig. 2.1 illustrates that by indirectly activating the ubiquitin-conjugating enzyme (UbE) which labels cyclin subunits for destruction, active MPF stimulates its own destruction. The Intermediary enzyme (IE) adds a delay to the signal, which makes this a potentially unstable negative feedback loop [3].

2.3 Mathematical Model

To convert the biochemical regulatory system into a system of mathematical equations, Novak and Tyson assumed that the chemical reactions take place in a more-or-less homogeneous chemical solution. Looking at the biochemical model (Fig. 2.1), the equation for the concentration of free cyclin would be derived by the following reasoning:

$$\begin{pmatrix} time-rate-of-change \\ of\ free\ cyclin\ concentration \end{pmatrix} = \begin{pmatrix} rate\ of\ cyclin \\ synthesis \end{pmatrix} - \begin{pmatrix} rate\ of\ cyclin \\ degradation \end{pmatrix} - \begin{pmatrix} rate\ of\ association\ of\ cyclin \\ with\ Cdc2\ monomers \end{pmatrix}.$$

Consequently,

$$\frac{d[C]}{dt} = k_1[amino\ acids] - k_2[C] - k_3[C][Cdc2],$$

where k_1, k_2, and k_3 are proportionality (or rate) constants. The rate of cyclin synthesis is dependent on the pool of amino acids that is available, the rate of cyclin degradation on the amount of cyclin available, and the rate of association with Cdc2 monomers depends on the probability of a collision between the two species (namely, on the product of their concentrations). Similar equations can be written for the four dimers including MPF. An equation for the Cdc2 monomer could also be written, but since there is no degradation of the Cdc2 monomer, total Cdc2 remains constant ($\frac{d[Cdc2]}{dt} = 0$).

For the four regulatory enzymes (Cdc25, IE, UbE, and Wee1), Michaelis-Menten rate laws are used [4]. The Michaelis-Menten rate law,

$$\begin{pmatrix} rate\ of\ loss \\ of\ substrate\ S \end{pmatrix} = \frac{V_{max}S}{K_m+S},$$

incorporates the effect of enzyme-saturation by excess substrate. The rate of reaction increases only up to some limiting value (V_{max}) which depends upon the total enzyme concentration. When $S = K_m$, $rate = \frac{1}{2}V_{max}$ (see Fig. 2.2).

Let us derive the rate equation for [Cdc25P], the concentration of the phosphorylated form of [Cdc25]. Looking at part B of the biochemical mechanism (Fig. 2.1), we see that

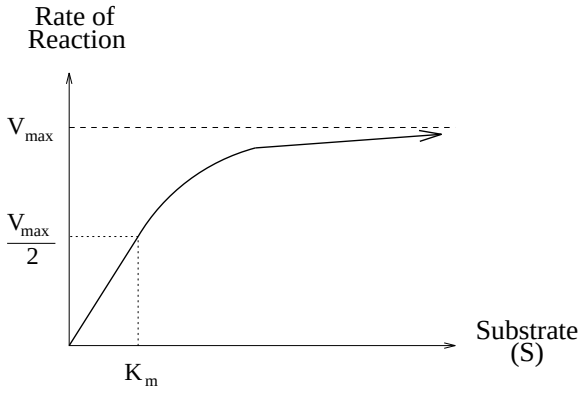

Figure 2.2: Michaelis-Menten Kinetics.

[Cdc25P] is obtained when MPF phosphorylates [Cdc25] (step a in the biochemical model). On the other hand, [Cdc25P] is lost by being dephosphorylated by a phosphatase [PPase] which is represented by step b. Using Michaelis-Menten kinetics to describe the kinase and phosphatase reactions, we arrive at the following rate equation:

$$\frac{d[Cdc25P]}{dt} = \frac{k_a[MPF]([total\ Cdc25] - [Cdc25P])}{K_a + [total\ Cdc25] - [Cdc25P]} - \frac{k_b[PPase][Cdc25P]}{K_b + [Cdc25P]},$$

where $[Cdc25] = [total\ Cdc25] - [Cdc25P]$ and the phosphorylated form of [Cdc25] is the more active form.

In this manner, Novak and Tyson derived the following equations to model the cell cycle engine:

$$
\begin{aligned}
\frac{d[C]}{dt} &= k_1[amino\ acids] - k_2[C] - k_3[C][Cdc2] \\
\frac{d[YT]}{dt} &= k_{PP?}[MPF] - (k_{wee} + k_{CAK} + k_2)[YT] + k_{25}[MPF] + k_3[C][Cdc2] \\
\frac{d[PYT]}{dt} &= k_{wee}[YT] - (k_{25} + k_{CAK} + k_2)[PYT] + k_{PP?}[PYTP] \\
\frac{d[PYTP]}{dt} &= k_{wee}[MPF] - (k_{PP?} + k_{25} + k_2)[PYTP] + k_{CAK}[PYT] \\
\frac{d[MPF]}{dt} &= k_{CAK}[YT] - (k_{PP?} + k_{wee} + k_2)[MPF] + k_{25}[PYTP] \\
\frac{d[Cdc25P]}{dt} &= \frac{k_a[MPF](\text{[total Cdc25] - [Cdc25P]})}{K_a + \text{[total Cdc25] - [Cdc25P]}} - \frac{k_b[PPase][Cdc25P]}{K_b + [Cdc25P]} \\
\frac{d[Wee1P]}{dt} &= \frac{k_e[MPF](\text{[total Wee1] - [Wee1P]})}{K_e + \text{[total Wee1] - [Wee1P]}} - \frac{k_f[PPase][Wee1P]}{K_f + [Wee1P]} \\
\frac{d[IEP]}{dt} &= \frac{k_g[MPF](\text{[total IE] - [IEP]})}{K_g + \text{[total IE] - [IEP]}} - \frac{k_h[PPase][IEP]}{K_h + [IEP]} \\
\frac{d[UbE^*]}{dt} &= \frac{k_c[IEP](\text{[total UbE] - [UbE}^*\text{]})}{K_c + \text{[total UbE] - [UbE}^*\text{]}} - \frac{k_d[\text{anti-IE}][UbE^*]}{K_d + [UbE^*]}.
\end{aligned}
$$

There are also three rate functions k_{25}, k_{wee}, and k_2 that are defined by the following equations:

$$
\begin{aligned}
k_{25} &= V_{25'}([total\ Cdc25] - [Cdc25P]) + V_{25''}[Cdc25P] \\
k_{wee} &= V_{Wee'}[Wee1P] + V_{Wee''}([total\ Wee1] - [Wee1P]) \\
k_2 &= V_{2'}([total\ UbE] - [UbE^*]) + V_{2''}[UbE^*].
\end{aligned}
$$

2.4 Previous Results from the Mathematical Model

The mathematical model described in Sec. 2.4 has 31 parameters (18 rate constants and 13 characteristic concentrations) that need to be specified before the differential equations

can be solved. Novak and Tyson specified the following basal set of rate parameters for simulations of oocyte extracts.

These parameters are dimensionless:

$K_a/[total\ Cdc25] = 0.1$ $K_b/[total\ Cdc25] = 0.1$ $K_c/[total\ UbE] = 0.01$
$K_d/[total\ UbE] = 0.01$ $K_e/[total\ Wee1] = 0.3$ $K_f/[total\ Wee1] = 0.3$
$K_g/[total\ IE] = 0.01$ $K_h/[total\ IE] = 0.01.$

These parameters have units min^{-1}

$k_1[AA]/[total\ Cdc2] = 0.1$ $k_3[total\ Cdc2] = 1.0$ $V_{2'}[total\ UbE] = 0.015$
$V_{2''}[total\ UbE] = 1.0$ $V_{25'}[total\ Cdc25] = 0.1$ $V_{25''}/[total\ Cdc25] = 2.0$
$V_{wee'}[total\ Wee1] = 0.1$ $V_{wee''}[total\ Wee1] = 1.0$ $k_{CAK} = 0.25$
$V_{PP?} = 0.025$
$k_a[total\ Cdc2]/[total\ Cdc25] = 1.0$ $k_b[PPase]/[total\ Cdc25] = 0.125$
$k_c[total\ IE]/[total\ UbE] = 0.1$ $k_d[antiIE]/[total\ UbE] = 0.095$
$k_e[total\ Cdc2]/[total\ Wee1] = 1.33$ $k_f[PPase]/[total\ Wee1] = 0.1$
$k_g[total\ Cdc2]/[total\ IE] = 0.65$ $k_h[PPase]/[total\ IE] = 0.087.$

Using this set of parameters, Novak and Tyson simulated in quantitative detail the findings of Solomon et al. on cyclin-induced activation of MPF [5], Felix et al. on MPF activation of cyclin degradation [6], Murray and Kirschner on MPF oscillations in oocyte extract [7], and Dasso and Newport on mitotic block by unreplicated DNA [8]. The model also gave new insight into the significance of thresholds, time-lags, and the role of tyrosine phosphorylation in Xenopus oocyte extracts and intact embryos. For more detailed information on their findings, see [3].

Chapter 3

Bifurcation Theory

3.1 Introduction

Before we discuss bifurcation theory, we need to look at some definitions and general results from the theory of differential equation. As can be seen from the previous chapter, we will be looking at a nonlinear, autonomous, first order system of ordinary differential equations of the form:

$$\dot{\mathbf{x}} = \mathbf{F}(\mathbf{x}; \mathbf{P}),$$

with initial condition

$$x_1(t_0) = x_1^0, x_2(t_0) = x_2^0, ..., x_n(t_0) = x_n^0,$$

where $\mathbf{x} \in \mathbf{R}^n$ is a vector of state variables and $\mathbf{P} \in \mathbf{R}^m$ is a vector of control parameters. The vector function $\mathbf{F}$ is defined as the map $\mathbf{F}$: $\mathbf{R}^n \times \mathbf{R}^m \rightarrow \mathbf{R}^n$. The following theorem ensures local existence and uniqueness of a solution for the above system [9, Theorem 7.1].

Theorem 3.1 (Existence and uniqueness) *Let each of the functions $f_1, \ldots, f_n$ and the partial derivatives $\frac{\partial f_1}{\partial x_1}, \ldots, \frac{\partial f_1}{\partial x_n}, \ldots \frac{\partial f_n}{\partial x_1}, \ldots, \frac{\partial f_n}{\partial x_n}$ be continuous in a region R of $x_1\ x_2\ \ldots x_n$ space containing the point $(x_1^0, x_2^0, \ldots, x_n^0)$. Then there exists an interval $\mid t - t_o \mid < h$ in which there exist a unique solution $x_1 = \phi_1(t), \ldots, x_n = \phi_n(t)$ of the above system of differential equations, which also satisfies the initial condition.*

The condition that the functions $f_1, \ldots, f_n$ and their derivatives be continuous is sufficient but not necessary. Since we will deal only with C^1 functions, this form of the existence-uniqueness theorem for ODEs is appropriate.

Fixed Points and Stability

An important class of solutions of differential equations are called *fixed points* or *steady states*. Fixed points are defined by the vanishing of the vector field (i.e., $\mathbf{F(x;P) = 0}$). Fixed points and their stability can relay important information about the solution of any system. Assuming solutions exist on $[t_0, \infty]$, we will be using the following definitions of stability:

A solution $\phi(t)$ is said to be *attracting* if there is a $\delta > 0$ such that for any other solution $\mathbf{x}$(t), the $\lim_{t\to\infty} \parallel \phi(t) - \mathbf{x}(t) \parallel \to 0$ whenever $\parallel \phi(t_0) - \mathbf{x}(t_0) \parallel < \delta$ (i.e., all trajectories that start near $\phi(t)$ approach it as $t \to \infty$).

A solution $\phi(t)$ is said to be *Lyapunov stable* if for any $\epsilon > 0$ there is a $\delta > 0$ such that for any other solution $\mathbf{x}$(t), $\parallel \phi(t) - \mathbf{x}(t) \parallel < \epsilon$ whenever t $\geq t_o$ and $\parallel \phi(t_o) - \mathbf{x}(t_o) \parallel < \delta$. (i.e., all trajectories that start sufficiently close to $\phi(t)$ remain close to $\phi(t)$ for all time).

We will call a solution *asymptotically stable* if it is both Lyapunov stable and attracting. We will call a solution *neutrally stable* if it is Lyapunov stable but not attracting. We will call a solution *unstable* if it is neither Lyapunov stable nor attracting.

The first line of attack in dealing with nonlinear systems is to find the fixed points and linearize the system at these points. Stability of the linearized system is defined in the above way. Stability of a linearized system need not imply stability of the original nonlinear system. For a certain class of fixed points though, called *hyperbolic*, the local behavior does carry over from the linearized system to the original nonlinear system. Therefore, with this in mind, we note that the given nonlinear system $\dot{\mathbf{x}} = \mathbf{F}(\mathbf{x}; \mathbf{P})$ with fixed point $\bar{\mathbf{x}}$, can be linearized about $\bar{\mathbf{x}}$ and the linear system will have the form

$$\dot{\mathbf{y}} = D_x\mathbf{F}(\bar{\mathbf{x}}; \mathbf{P})\mathbf{y}$$

where $D_x\mathbf{F} = [\partial f_i/\partial x_j]$ is the Jacobian matrix consisting of first partial derivatives. If $D_x\mathbf{F}(\bar{\mathbf{x}}; \mathbf{P})$ has no eigenvalues with zero real part, then $\bar{\mathbf{x}}$ is called a *hyperbolic* fixed point. If one or more of the eigenvalues of the Jacobian matrix has zero real part then the fixed point is called *nonhyperbolic*. For some nonhyperbolic fixed points, stability cannot be determined by the linearized system alone.

There are three types of hyperbolic fixed points: *sources, sinks*, and *saddle points*. If a

fixed point is asymptotically stable (all eigenvalues of $D_x\mathbf{F}$ have negative real parts), it is called a *sink*. If all the eigenvalues associated with the sink are real, then it is called a *stable node*, otherwise it is called a *stable focus*. If all the eigenvalues of the Jacobian matrix have positive real parts, the fixed point is unstable and is called a *source*. A source with only real eigenvalues is called an *unstable node*, otherwise it is called an *unstable focus*. If the eigenvalues of $D_x\mathbf{F}$ have both negative and positive real parts, then the fixed point is unstable and is called a *saddle point*.

In the nonhyperbolic case, if one or more of the eigenvalues of $D_x\mathbf{F}$ have positive real parts, the nonhyperbolic fixed point is unstable. If some of the eigenvalues of $D_x\mathbf{F}$ have negative real parts and the rest have zero real parts, then the stability of the fixed point cannot necessarily be determined. If there are only purely imaginary eigenvalues, the fixed point is called a *center*.

The *Hartman-Grobman Theorem* [13, Chapter 3], [14, Chapter 2] (for hyperbolic fixed points) and the *Shoshitcishvili Theorem* [13, Chapter 6] (for nonhyperbolic fixed points), are two theorems by which the following conclusions can be drawn [10, Sec. 2.1.2]:

1. If the fixed point of the linear system is asymptotically stable, then the corresponding fixed point for the nonlinear system is stable.
2. If the fixed point of the linear system is unstable, then the corresponding fixed point for the nonlinear system is unstable.
3. In the case of neutrally stable fixed points (including centers), nonlinear analysis is necessary to determine the stability of the fixed point.

Periodic Solutions and Floquet Multipliers

Another type of important solution to differential equations is a *periodic solution* or *periodic orbit*. A solution $\mathbf{x}$(t) is a periodic solution with least period T_0 if $\mathbf{x}(t + T_0) = \mathbf{x}(t)$ and $\mathbf{x}(t + T) \neq \mathbf{x}(t)$ for any $0 < T < T_0$. A periodic solution is called a limit cycle if it is an isolated periodic solution. In other words, neighboring trajectories are not closed; they spiral either toward or away from the limit cycle. A limit cycle corresponds to an isolated closed orbit in the phase space. Unless otherwise noted, the periodic solutions that we will see in the *Xenopus* model are limit cycles.

Similar to eigenvalues of fixed point solutions, the stability of periodic solutions can be determined by looking at the Floquet multipliers. Consider again the system of differential

equations

$$\dot{\mathbf{x}} = \mathbf{F}(\mathbf{x}; \mathbf{P})$$

and let $\bar{\mathbf{x}}$(t)=$\bar{\mathbf{x}}(t + T_0)$ be a periodic solution at $\bar{\mathbf{P}}$ lying on a closed orbit γ. Linearizing the differential equation about γ, we obtain the system

$$\dot{\mathbf{y}} = D_x\mathbf{F}(\bar{\mathbf{x}}; \bar{\mathbf{P}})\mathbf{y}$$

where $D_x\mathbf{F}(\bar{\mathbf{x}};\bar{P})$ is an $n \times n$ time-dependent matrix of period T_0. The $n-$dimensional linear system has n linearly independent solutions $\mathbf{y}_i$, $i = 1, \ldots, n$. When these n solutions are expressed in columns, they form a $n \times n$ matrix which is called a *fundamental matrix* and denoted by Φ.

The following classic theorem with proof can be found in [11, Theorem 4.2].

Theorem 3.2 *If $\Phi(t)$ is a fundamental matrix for a linear periodic system then so is $\Phi(t+T_0)$. Morever, corresponding to every Φ there exists a nonsingular matrix $\mathbf{Z}$ which is also periodic with period T_0 and a constant matrix $\mathbf{R}$ such that*

$$\mathbf{\Phi}(t) = \mathbf{Z}(t)e^{t\mathbf{R}}, \mathbf{Z}(t) = \mathbf{Z}(t + T_0).$$

Therefore, if we choose $\Phi(0)$=$\mathbf{Z}(0)$=$\mathbf{I}$ then

$$\mathbf{\Phi}(T_0) = \mathbf{Z}(T_0)e^{T_0\mathbf{R}} = \mathbf{Z}(0)e^{T_0\mathbf{R}} = e^{T_0\mathbf{R}}.$$

It follows that the behavior of solutions in the neighborhood of γ is determined by the eigenvalues of the constant matrix $e^{T_0\mathbf{R}}$. These eigenvalues are called Floquet multipliers. For a full derivation, including relations to Poincare maps, see [12, Sec. 1.5] or [10, Sec. 3.2-3.3].

It is important to note that the multiplier associated with perturbations along the periodic solution of an autonomous system is always unity. Stability of the periodic orbit is then determined by the remaining $n - 1$ Floquet multipliers. A periodic solution is known as a *hyperbolic* periodic solution if only one Floquet multiplier is located on the unit circle in the complex plane. A hyperbolic periodic solution can be either stable or unstable. A hyperbolic periodic solution is stable if there are no Floquet multipliers outside the unit circle. This solution is called a *stable limit cycle* or *periodic attractor* since neighboring trajectories are attracted to the periodic orbit. If one or more of the Floquet multipliers lie outside the unit circle, the hyperbolic periodic solution is unstable and all neighboring trajectories are repelled in positive time. This solution is known as an *unstable limit cycle*

or *periodic repeller*. When some of the Floquet multipliers associated with an unstable limit cycle lie inside the unit circle, the periodic solution is called an *unstable limit cycle of the saddle type*.

If two or more Floquet multipliers lie on the unit cycle, the periodic solution is called a *nonhyperbolic* periodic solution. If one or more of the Floquet multipliers lie outside the unit cycle, then the nonhyperbolic periodic solution is unstable. If none of the associated Floquet multipliers lie outside the unit circle, then nonlinear analysis is needed to determine the stability of the nonhyperbolic periodic solution.

Invariant Manifolds

We can represent $\mathbf{R}^n$ as the direct sum of three subspaces denoted $\mathbf{E}^s$, $\mathbf{E}^u$, and $\mathbf{E}^c$. We define these subspaces by the following:

$$\begin{aligned} \mathbf{E}^s &= span[v_1, v_2, \ldots, v_s] \\ \mathbf{E}^u &= span[v_{s+1}, v_{s+2}, \ldots, v_{s+u}] \\ \mathbf{E}^c &= span[v_{s+u+1}, v_{s+u+2}, \ldots, v_{s+u+c}], \end{aligned}$$

where $s + u + c = n$. $[v_1, v_2, \ldots, v_s]$ are the eigenvectors (could be generalized if there are repeated eigenvalues) of the Jacobian matrix corresponding to the eigenvalues having negative real parts. $[v_{s+1}, v_{s+2}, \ldots, v_{s+u}]$ are the (generalized) eigenvectors corresponding to the eigenvalues having positive real parts. $[v_{s+u+1}, v_{s+u+2}, \ldots, v_{s+u+c}]$ are the (generalized) eigenvectors corresponding to the eigenvalues having zero real part. The subspaces $\mathbf{E}^s$, $\mathbf{E}^u$, and $\mathbf{E}^c$ are called *invariant subspaces* of the linear system since a solution of the linear system starting in one of these subspaces remains in the subspace for all time. The subspace $\mathbf{E}^s$ is called a *stable subspace* or *manifold*, and solutions that lie within it converge to the fixed point as $t \to \infty$. The subspace $\mathbf{E}^u$ is called an *unstable subspace* or *manifold*, and solutions that lie within this subspace diverge from the fixed point as $t \to \infty$. The subspace $\mathbf{E}^c$ is called a *center subspace* or *manifold* and solutions within the center manifold do not converge to the fixed point nor diverge from it as $t \to \infty$. The nonlinear system has subspaces or manifolds called $\mathbf{W}^s$, $\mathbf{W}^u$, and $\mathbf{W}^c$. These subspaces are tangent to the respective linear subspaces at the fixed point. For the nonlinear system, manifolds are only guaranteed to exist in a neighborhood of the fixed point and therefore they are *local invariant manifolds*. Simply put, all initial conditions whose trajectories approach the fixed point asymptotically make up the stable manifold. Similiar statements can be made for the unstable and center manifolds.

3.2 Terminology and Concepts of Bifurcation Theory

A *bifurcation* is a qualitative change in the behavior of solutions as one or more parameters are varied. The parameter values at which these changes occur are called *bifurcation points*. If the qualitative change occurs in a neighborhood of a fixed point or periodic solution, it is called a *local bifurcation*. Any other qualitative change that occurs is considered a *global bifurcation*. Another way to think of a bifurcation is the following: As one or more control parameters are varied, a fixed point may become nonhyperbolic for a certain parameter value. If the state-space portraits are qualitatively different before and after this location, then this point is called a bifurcation point and the qualitative change is called a bifurcation [10, pg.70].

We discussed the stability of solutions of a system of ordinary differential equations in the previous section. It is also possible to define a concept of structual stability of the system itself. To see the structural stability of a system of ODEs, we look at the qualitative features of the full set of orbits of the system. The term orbit includes: fixed points, periodic orbits, homoclinic orbits (closed orbits that lead to the same saddle point in forward and reverse time), and heteroclinic orbits (trajectories that lead to different saddle points in forward or reverse time). A system is said to be *structurally stable* if for any small change in parameter space, the qualitative features of the new system are equivalent to the initial system. We can summarize with the following observations (for extensive treatment, see [13, Chapter 3]):

1. Orbits and therefore vector fields are structurally stable in the vicinity of hyperbolic fixed points (this is a result of Hartman-Grobman Theorem [13, Chapter 3],[14, Chapter 2]).

2. In the vicinity of bifurcation points, the orbits and therefore the associated vector field is structurally unstable. This statement is fairly obvious since the state space portraits are qualitatively different before and after a bifurcation as mentioned above.

The *codimension* of a bifurcation is the smallest dimension of parameter space for which the bifurcation occurs. (If a bifurcation is codimension-n, then at least n independent parameters must be specified for the bifurcation to occur).

The *normal form* or *model system* of a bifurcation is the simplest system that exhibits the change of orbit structure, and the original systems of equations can always be transformed into the normal form close to the local bifurcation point. This simplification can be achieved by several methods (e.g. see [10, Sec. 2.3.4-2.3.6] or [12, Sec. 3.3]). Since local bifurcations can only happen at nonhyperbolic fixed points, one might guess that looking

at the eigenvectors in $\mathbf{E}^c$ (the center manifold) would give an idea of the dynamics near the bifurcation point. This idea is supported by the center manifold theorem (e.g., [12, Sec. 3.2]). The center manifold theorem restricts the attention to the flow within the center manifold and the use of normal forms simplifies the system of equations (or vector field) on the center manifold. Every system, no matter how big, can be simplified to the normal form at the bifurcation point. By looking at the normal form, we can see generic qualitative behavior of the flows of the specific type of local bifurcation. This is very helpful when dealing with systems of higher dimensions (like the *Xenopus* model).

3.3 Codimension-1 Bifurcations

We are now ready for our 'Dictionary' of bifurcations seen in the *Xenopus* model.

Saddle-Node : SN

The saddle-node bifurcation, also called a *fold* or *turning point*, is the simplest way that fixed points are created or destroyed. As a parameter is varied, two fixed points approach each other, collide, and are destroyed. As the parameter is varied from the opposite direction, one sees the simultaneous birth of a pair of fixed points. In order for a saddle-node bifurcation to occur at the point $(\mathbf{x_b}; \alpha_\mathbf{b})$ (where α is the parameter being varied), the following two conditions are necessary, but not sufficient:

1. $\mathbf{F}(\mathbf{x_b}; \alpha_\mathbf{b}) = \mathbf{0}$
2. $D_x\mathbf{F}$ must have precisely one zero eigenvalue, while the rest of the eigenvalues have nonzero real parts at $(\mathbf{x_b}; \alpha_b)$.

The first condition implies that the solution is a fixed point while the second condition implies that the fixed point is nonhyperbolic.

For higher dimensions, the two fixed points that collide are usually a saddle and a node. In general, a saddle-node bifurcation involves two fixed points whose stable manifolds have dimensions that differ by one. The normal form for a saddle-node bifurcation in the plane is

$$\dot{x} = \alpha + x^2.$$

Kuznetsov concludes that in a strong sense this describes the saddle-node bifurcation in a

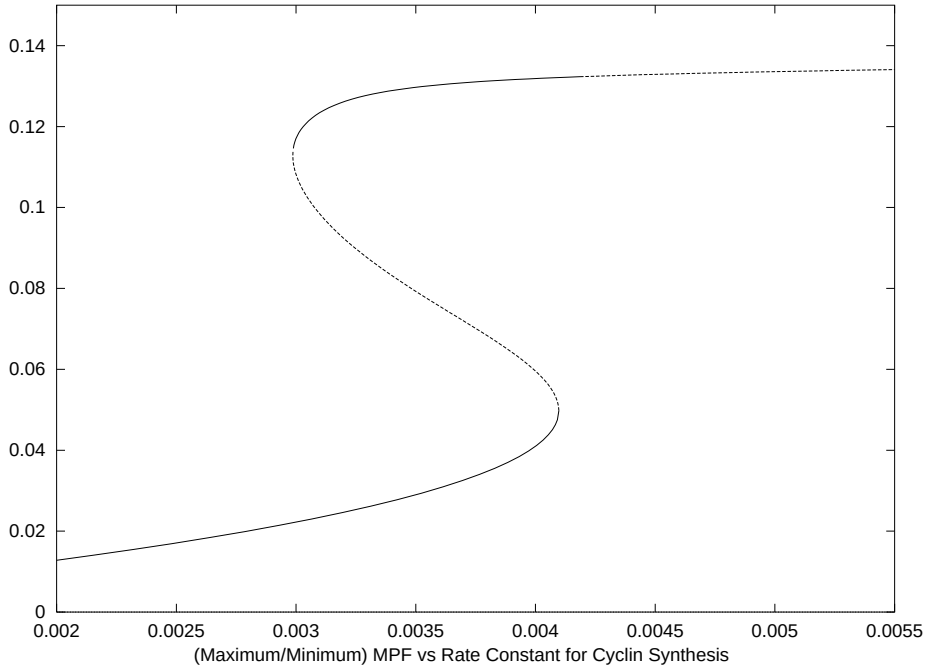

The dotted line represents unstable fixed points and the solid line represents stable fixed points. There are two saddle-node bifurcations pictured: rate constant for cyclin synthesis approximately 0.0029 and 0.0041. If a second parameter is varied these two bifurcation move apart or come together to form a cusp in the two parameter plane. This resulting codimension-2 bifurcation (Cusp Bifurcation) will be described in the next section. The change in stability on the upper branch, directly above the saddle-node is due to a Hopf bifurcation (see Fig. 3.4).

Figure 3.1: Saddle-Node Bifurcation in the *Xenopus* Model.

generic $n-$dimensional system (e.g., [15, Sec. 5.2]). See Fig. 3.1 for a pair of saddle-node bifurcations that are seen in the *Xenopus* model.

Hopf Bifurcation : H

A Hopf bifurcation causes a family of periodic orbits to branch from a curve of fixed points. The following are the conditions under which a Hopf bifurcation will occur at the point $(\mathbf{x_b}; \alpha_\mathbf{b})$ (e.g. [10, Sec. 2.3.1]):

1. $\mathbf{F}(\mathbf{x_b}; \alpha_\mathbf{b}) = \mathbf{0}$
2. $D_x\mathbf{F}$ has a pair of purely imaginary eigenvalues while the rest of the eigenvalues have nonzero real parts.
3. A pair of complex conjugate eigenvalues, $\lambda \pm i\omega$, $(\omega > 0)$ simultaneously cross the imaginary axis and proceed into the right half-plane as α varies across α_b, i.e. $\frac{\partial \lambda}{\partial \alpha} \mid_{\alpha=\alpha_b} \neq 0$. This is referred to as the transversality condition.

When all three conditions are satisfied, a periodic solution of period $2\pi/\omega_b$ is born at $(\mathbf{x_b}; \alpha_\mathbf{b})$. There are two types of Hopf bifurcations: the *Supercritical Hopf Bifurcation* and *Subcritical Hopf Bifurcation*. We will look at each separately.

Supercritical Hopf Bifurcation : SpH

The normal form for the generic 2-dimensional supercritical Hopf bifurcation is:

$$\dot{x} = \alpha x - y - x(x^2 + y^2)$$

$$\dot{y} = x + \alpha y - y(x^2 + y^2).$$

Locally (see Fig. 3.2 and Fig. 3.3), we will have a branch of stable fixed points (foci) on one side of the bifurcation point, and on the other side of the bifurcation point, a branch of unstable fixed points (foci) surrounded by a branch of stable periodic solutions. The following are two rules that hold in general for a supercritical Hopf bifurcation (e.g. [16, Sec. 2.8]):

1. The size of the periodic solution increases continuously from zero. The increase is proportional to $\sqrt{\alpha - \alpha_b}$ locally.

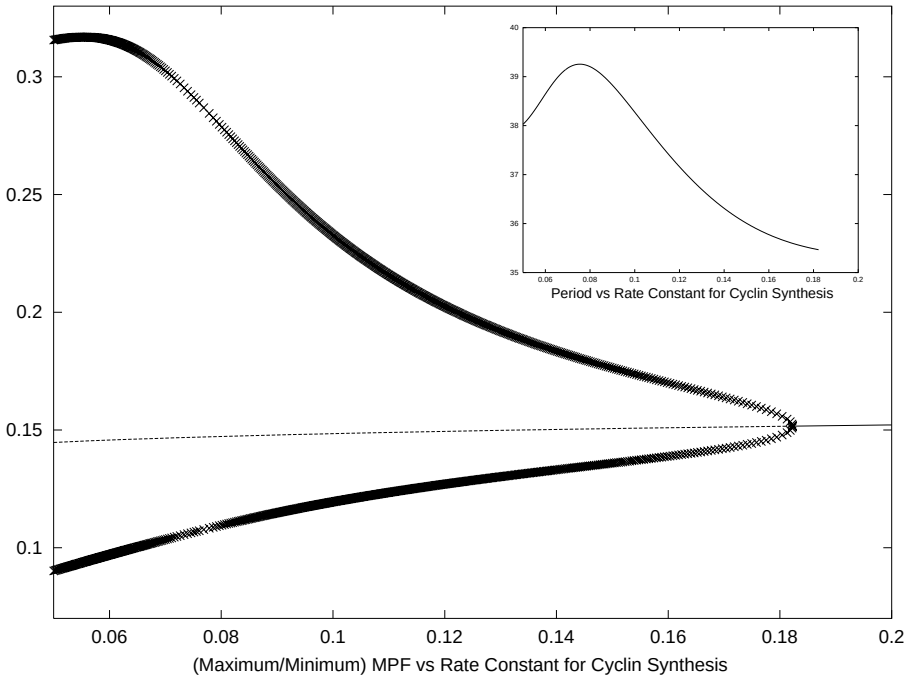

The solid line represents stable fixed points, the broken line represents unstable fixed points. There is a supercritical Hopf bifurcation at rate constant for cyclin synthesis approximately 0.18. At this point a branch of stable limit cycles begins and the fixed point changes stablity. The maximum and minimum of these limit cycles are represented, respectively, by the higher and lower curves of Xs that emanate from the SpH. The inlayed graph shows the period of the limit cyles. The period increases locally and then decreases for a short interval. The period begins increasing again until it reaches infinity and is destroyed via a SNIC bifurcation. See Fig. 3.9.

Figure 3.2: Supercritical Hopf Bifurcation in the *Xenopus* Model.

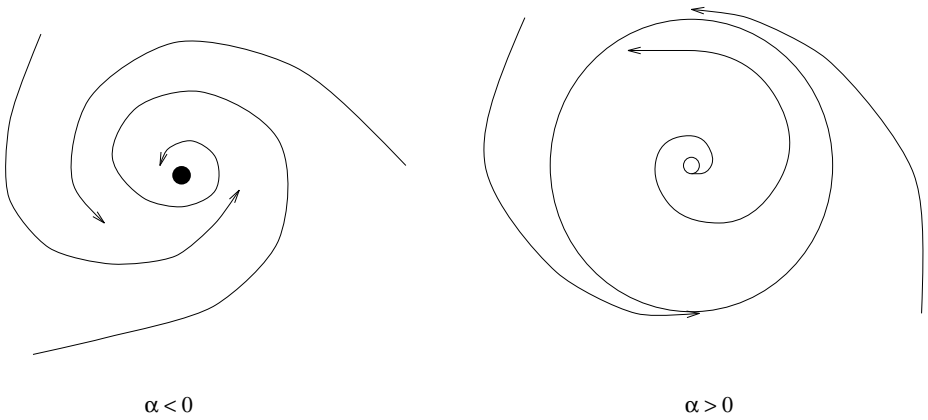

XY phase plane of the normal form for the supercritical Hopf bifurcation. A SpH bifurcation takes place at $\alpha = 0$. For $\alpha < 0$ there is a stable fixed point. For $\alpha > 0$ there is a stable limit cycle surrounding an unstable fixed point.

Figure 3.3: Phase Portrait of the Supercritical Hopf Bifurcation.

2. As mentioned previously, the frequency of the periodic solution is given approximately by $\omega_b = Im\lambda$ for α close to α_b: $T_0 = \frac{2\pi}{\omega_b} + A\sqrt{\alpha - \alpha_b}$, with A = constant.

Subcritical Hopf Bifurcation : SbH.

The normal form for a subcritical Hopf bifurcation is the same as for the supercritical case except the signs of the nonlinear terms change from negative to positive. Locally, on one side of the bifurcation, we will have a branch of stable fixed points surrounded by branch of unstable periodic solutions. As the parameter is varied through the bifurcation point, we come out on the other side with only a branch of unstable fixed points left. By looking at the phase portrait of the normal form, Fig. 3.5, we can see why this bifurcation is more interesting than the supercritical case. For $\alpha < 0$ there is one attractor, a stable fixed point which is surrounded by an unstable limit cycle. As α increases, the unstable limit cycle loses amplitude and converges to the fixed point. At $\alpha = 0$ the subcritical Hopf bifurcation occurs. The amplitude of the unstable limit cycle goes to zero, collapses to the origin, and renders the fixed point unstable. For $\alpha > 0$, solutions that before were confined near the stable fixed point are now forced to find another attractor: a fixed point, stable limit cycle, infinity, or a chaotic attractor. In a biochemical system the attractor is usually a stable limit cycle, as seen in the *Xenopus* model (Fig. 3.4).

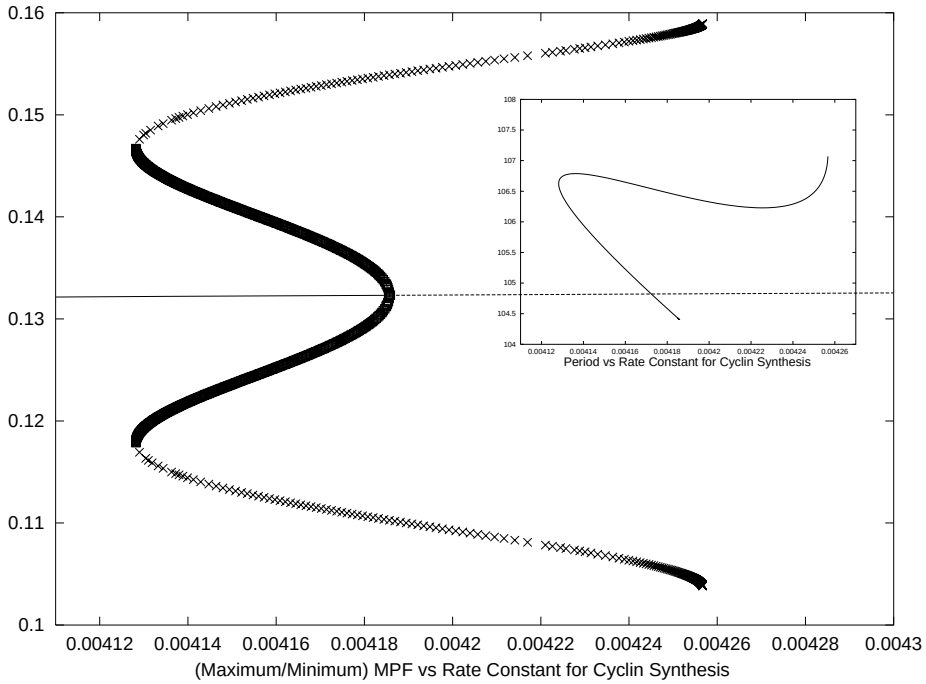

The solid line represents stable fixed points, the broken line represents unstable. There is a subcritical Hopf bifurcation at rate constant for cyclin synthesis approximately 0.00418. At this point a branch of unstable limit cycles begins. The maximum and minimum of these limit cycles are represented, respectively, by the higher and lower curves of boxes that emanate from the SbH. At rate of cyclin synthesis approximately 0.00413, this branch of unstable limit cycles are destroyed as they coalesce with a branch of stable limit cycles (X) at a cyclic fold bifurcation. In the inlay, we see the period of both the stable and unstable limit cycles. The period continues to increase as these limit cycles go through another cyclic fold bifurcation and end with the period going to infinity as the limit cycles become homoclinic to a saddle point at a saddle-loop bifurcation. See Fig. 3.7.

Figure 3.4: Subcritical Hopf Bifurcation in the *Xenopus* Model.

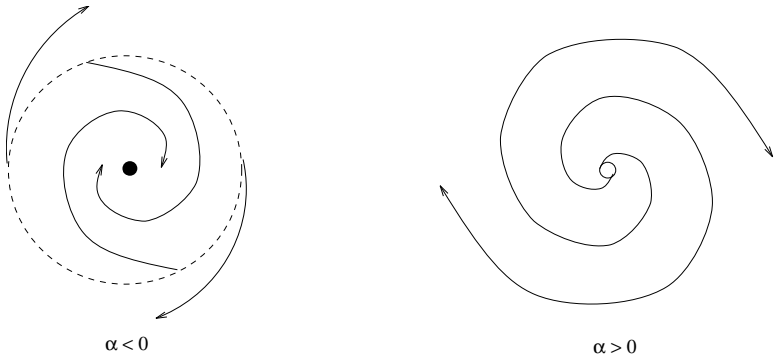

XY phase plane of the normal form for the subcritical Hopf bifurcation. A SbH bifurcation takes place at $\alpha = 0$. For $\alpha < 0$ there is an unstable limit cycle (represented by the dotted line) surrounding a stable fixed point. At $\alpha > 0$ we are left with an unstable steady state. Nearby trajectories that were confined close to the orgin by the unstable orbit are now drawn to some type of distant attractor.

Figure 3.5: Phase Portrait of the Subcritical Hopf Bifurcation.

A SbH also exhibits a property known as *hysteresis*. Hysteresis is the lack of reversibility as a parameter is increased or decreased. This can be seen in Fig. 3.4. When the rate constant for cyclin synthesis is increased past the SbH (approximately 0.004185) and the large amplitude oscillations have begun, they cannot be stopped by bringing the parameter back down to 0.004185. It must be futher decreased to 0.004125 in order for these large amplitude oscillations to be destroyed via a cyclic fold bifurcation, which we will consider next.

Cyclic Fold : CF

The cyclic fold bifurcation (also known as a *saddle-node of periodic orbits*) is similiar to the saddle-node bifurcation, except instead of fixed points, there are periodic orbits (or limit cycles) coming together. A branch of stable periodic solutions and a branch of unstable periodic solutions coalesce and are destroyed at the bifurcation point.

Looking at the Floquet multipliers at a cyclic fold bifurcation, there is one multiplier leaving or returning into (depending on the direction the parameter is varied) the unit circle on the complex plane through +1. Cyclic fold bifurcations are one of the ways that limit cycles can be born or destroyed. These bifucations can usually be observed, near subcritical Hopf bifurcations (See Fig. 3.4).

Saddle-Loop : SL

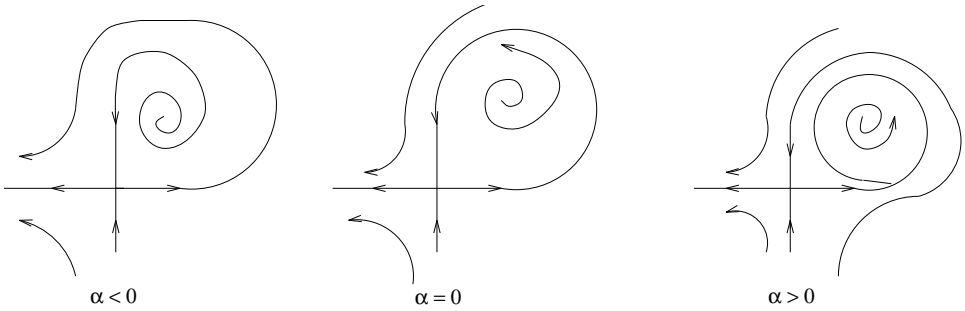

XY phase plane for the saddle-loop bifurcation. Looking at the figures from right to left, for $\alpha > 0$ we have a saddle point and a high period limit cycle. At $\alpha = 0$ a saddle-loop bifurcation takes place. At the bifurcation the period of the limit cycle has become infinite and the orbit is homoclinic to the saddle point. As the parameter is perturbed further so that $\alpha < 0$, the homoclinic orbit is broken and the limit cycles that were seen for $\alpha > 0$ cease to exist.

Figure 3.6: Phase Portrait of the Saddle-Loop Bifurcation.

The saddle-loop bifurcation, also known as a *homoclinic bifurcation*, terminates a family of limit cycles as the period of these cycles becomes infinite. There is more than one type of saddle-loop bifurcation. We will only be interested in the type that we see in the *Xenopus* model. Nayfeh looks at the following system:

$$\dot{x} = \lambda_1 x + f_1(x, y; \alpha)$$
$$\dot{y} = -\lambda_2 y + f_2(x, y; \alpha)$$

where f_1 and f_2 are $O(x^2 + y^2)$, $\lambda_1, \lambda_2 > 0$, and $\lambda_1, -\lambda_2$ are the eigenvalues of the Jacobian matrix. The following discussion regarding this system is found in [10, Sec. 1.8].

> The planar results discussed in this section are applicable to higher-dimensional systems without symmetry provided that the following conditions are satisfied. First, the system has an orbit homoclinic to a saddle point; that is, an orbit that approaches the saddle as $t \to \pm\infty$. Second, the eigenvalues of the Jacobian matrix associated with the saddle have a special structure. Out of all of the eigenvalues in the right-half of the complex plane, the closest to the imaginary axis is a real eigenvalue λ_1. And out of all of the eigenvalues in the left-half of the complex plane, the closest to the imaginary axis is a real eigenvalue $-\lambda_2$. Thus, the dynamics of the system near the homoclinic orbit can be reduced to that of a planar system because the eigenvalues λ_1 and $-\lambda_2$ determine how the homoclinic orbit approaches and leaves the saddle point.

The eigenvalues for saddle points in the *Xenopus* model always have the above structure and we do not have symmetry. Therefore we can think of the above system as the normal form

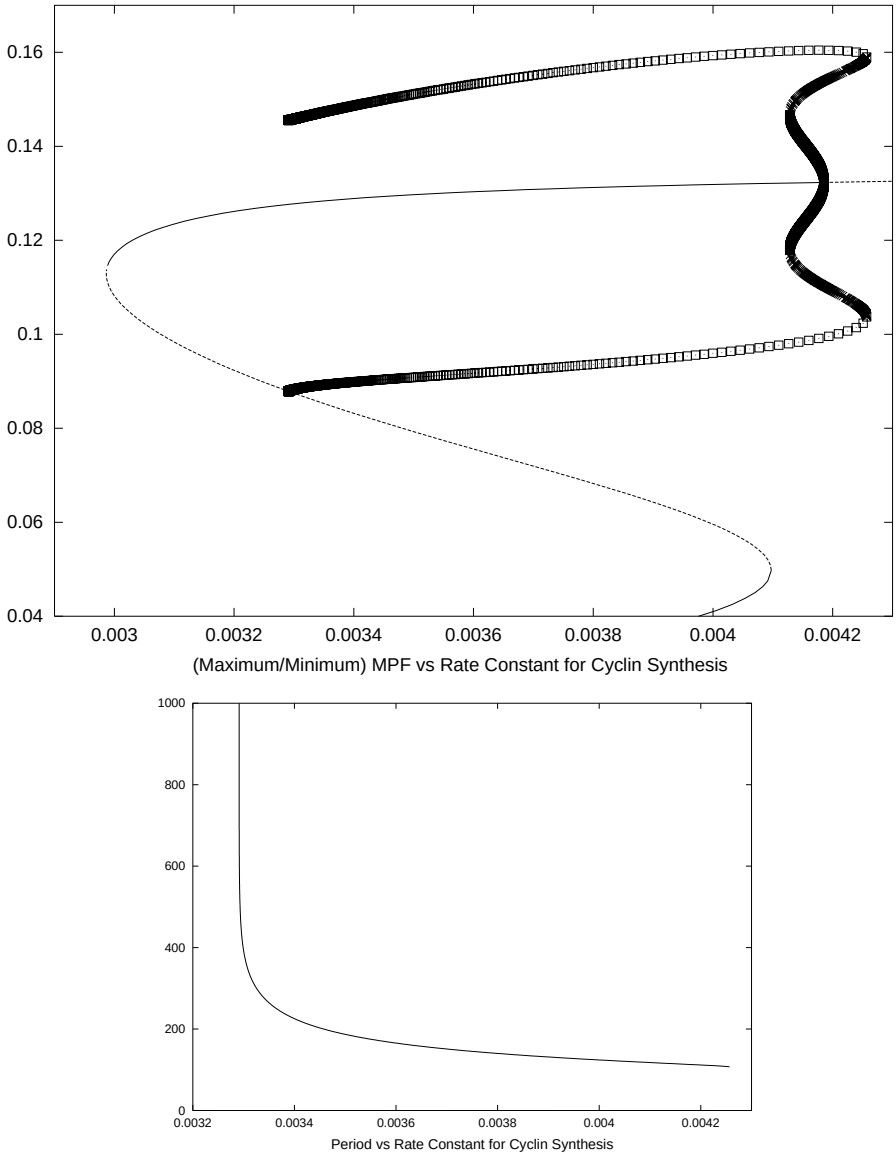

Continuation of Fig. 3.2. After a second cyclic fold bifurcation the limit cycles become unstable and remain that way as the period increases to infinity, and are destroyed at a saddle-loop bifurcation. The limit cycles become homoclinic to a saddle point that is between the two folds (rate constant for cyclin synthesis approximately 0.0033). The lower graph shows the period of the limit cycles as it becomes very large as the bifurcation point is approached.

Figure 3.7: Saddle-Loop Bifurcation in the *Xenopus* Model.

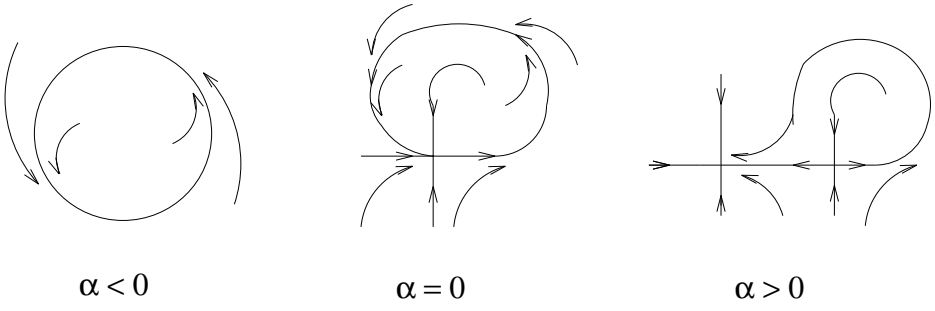

XY phase plane of the SNIC bifurcation. α is the bifurcation parameter. When $\alpha < 0$ we have a high period limit cycle. At $\alpha = 0$ a SNIC bifurcation takes place–a saddle-node appears, the period of the limit cycle becomes infinite, and the orbit becomes homoclinic to the saddle-node. As the parameter is perturbed further so that $\alpha > 0$, the homoclinic orbit is broken as the saddle and node separate, and the limit cycles that were seen for $\alpha < 0$ cease to exist.

Figure 3.8: Phase Portrait of the SNIC Bifurcation.

for the saddle-loop bifurcation found in the *Xenopus* model. Fig. 3.6 is the phase portrait for this normal form. Also see Fig. 3.7 for a saddle-loop bifurcation in the *Xenopus* model.

Saddle-Node on Invariant Circles : SNIC

As we will see, there is a codimension-2 saddle-node-loop bifurcation. In the unfolding of that bifurcation, we will see the need for something to describe the phenomenon of a limit cycle with infinite period being homoclinic to a saddle-node as only one parameter is varied. This is called a saddle-node on invariant circles bifurcation. See Fig. 3.14 and discussion of SNL for comparison. The phase portrait for the SNIC can be seen in Fig. 3.8. See Fig. 3.9 for this bifurcation in the *Xenopus* model.

3.4 Codimension-2 Bifurcations

Cusp : C

At a cusp bifurcation, three fixed points coalesce into one. A normal form for the cusp in

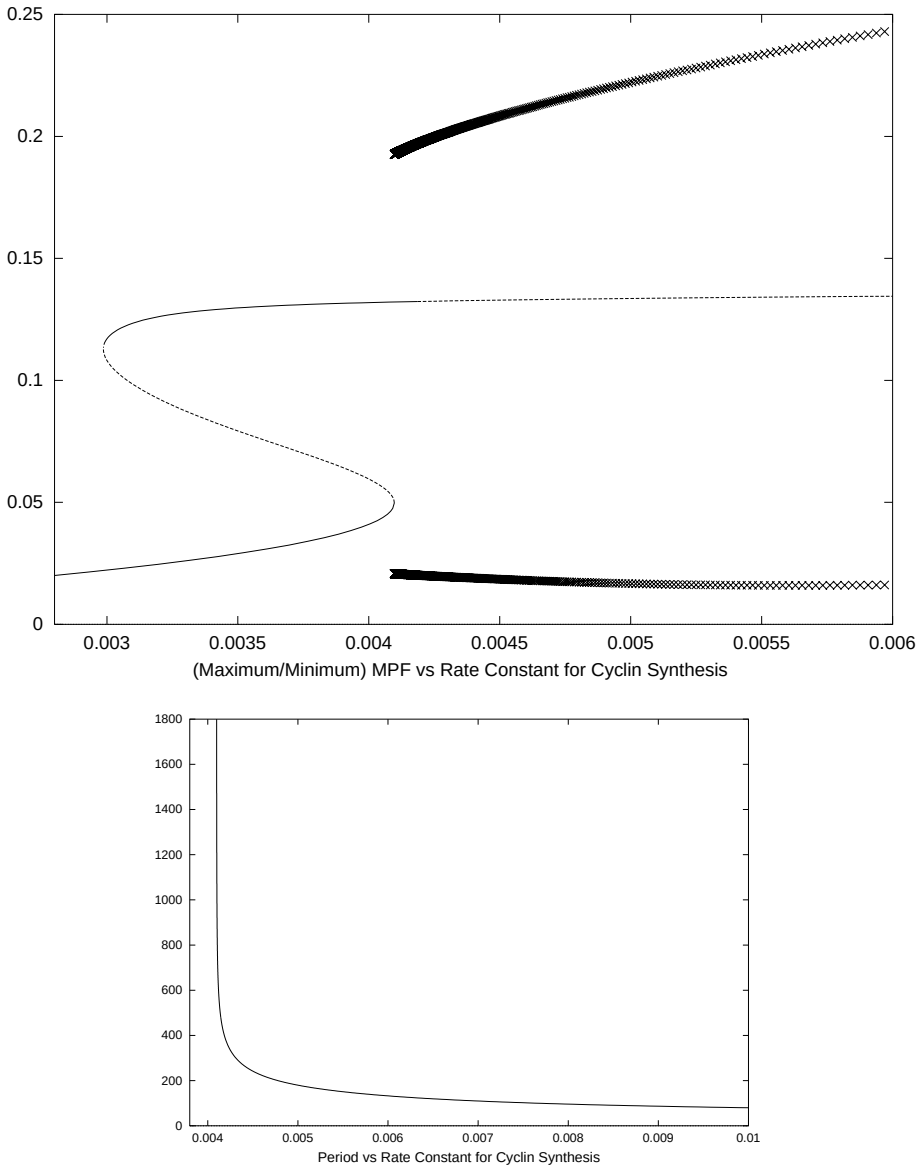

Continuation of limit cycles from SpH bifurcation seen in Fig. 3.2. The limit cycles have remained stable and the period has increased as the parameter (rate constant for cyclin synthesis) has been decreased. At approximately 0.0041, the period goes to infinity as the limit cycles become homoclinic to the saddle-node and are destroyed via a saddle-node loop bifurcation. The lower graph shows that the period, as the limit cycles approach the saddle-node, is going to infinity.

Figure 3.9: Saddle-Node on Invariant Circles Bifurcation in the *Xenopus* Model.

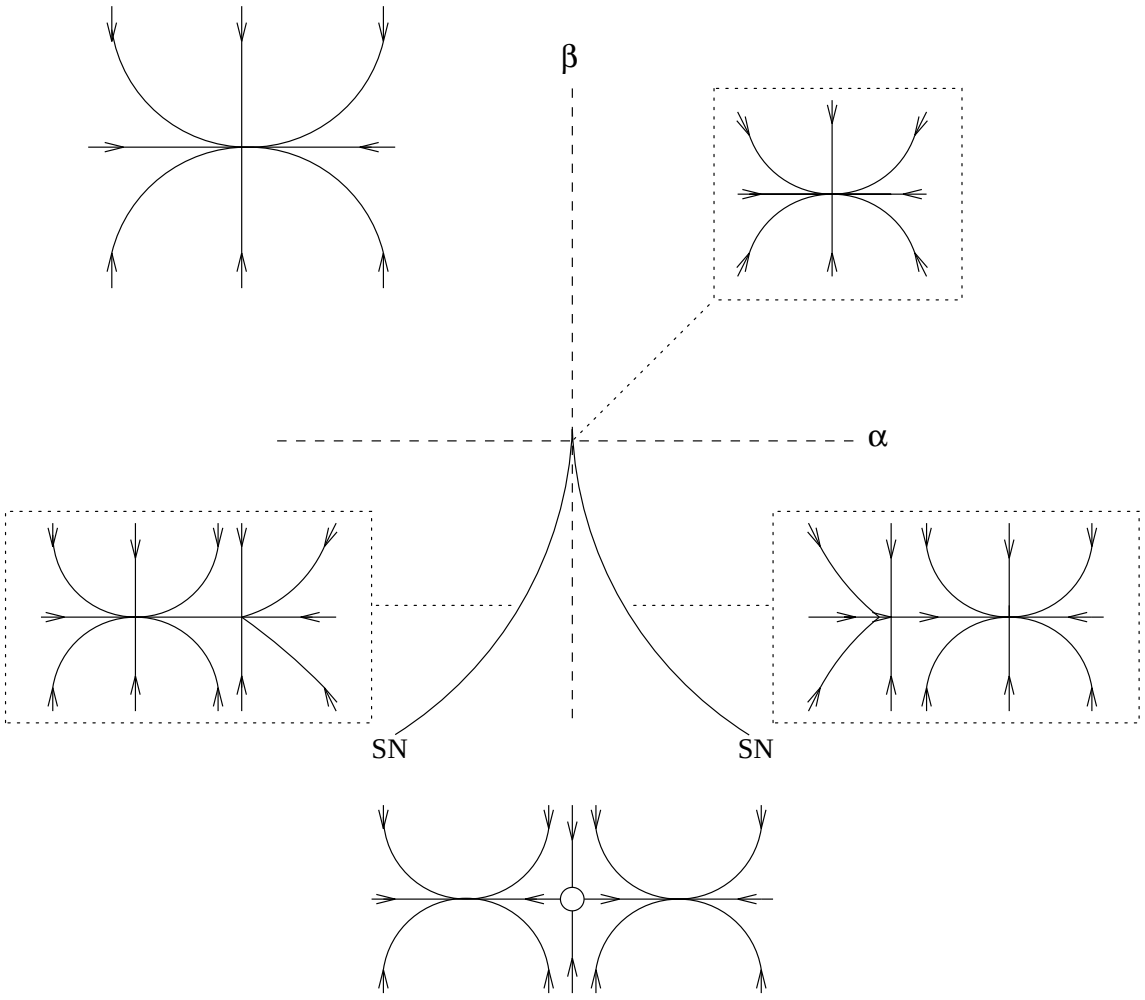

Two varieties depending on the stability of the nodes:(s,x,s)-pictured above, (u,x,u)-time reversal. Both are seen in the *Xenopus* model. Second is time reversal of the first (s=stable node, x=saddle, u=unstable node).

Figure 3.10: Unfolding of the Cusp Bifurcation on the Parameter Plane.

the plane is

$$\dot{x} = \alpha - \beta x - x^3$$
$$\dot{y} = \gamma y \, (\gamma \neq 0).$$

A cusp bifurcation occurs when the following conditions are satisfied:

1. A fixed point with a zero eigenvalue.
2. In the direction of the eigenvector coresponding to the zero eigenvalue, a second derivative of the vector field vanishes (e.g. [15, Sec. 8.1-8.2]).

If we look at the two parameter bifurcation diagram (Fig. 3.10), we will see two curves of saddle-node bifurcations meeting tangentially to form a semicubical parabola. The point at which the two curves meet is the cusp bifurcation. The resulting wedge divides the parameter plane into two regions. The region inside the wedge contains three fixed points and the region outside the wedge contains one fixed point. On the SN curves there are two fixed points. As one crosses either curve separating the regions, a saddle-node bifurcation takes place. Coming from inside the wedge, we see a saddle and node collide and disappear, leaving only one fixed point. As one approaches the cusp point from the inside region, all three fixed points merge together into one.

Degenerate Hopf : DH

A Hopf bifurcation can become degenerate if any one of the genericity conditions of Hopf's Theorem fails. An important type of degeneracy occurs when the coefficient of the r^3 term in the normal form of the Hopf bifurcation vanishes. This condition (plus the requirement that the r^5 coefficient not vanish) yields a codimension-2 bifurcation that is called a degenerate Hopf bifurcation (or, more precisely, a *Bautin* bifurcation). A normal form for the DH bifurcation in polar coordinates is:

$$\dot{r} = \alpha r + \beta r^3 - r^5$$
$$\dot{\theta} = 1.$$

At a DH, a cyclic fold curve collapses onto a curve of Hopf bifurcations. The two curves divide the plane into three different regions having zero, one, or two periodic orbits. Furthermore, a DH divides a Hopf bifurcation curve into two parts. For $\beta < 0$, the line of

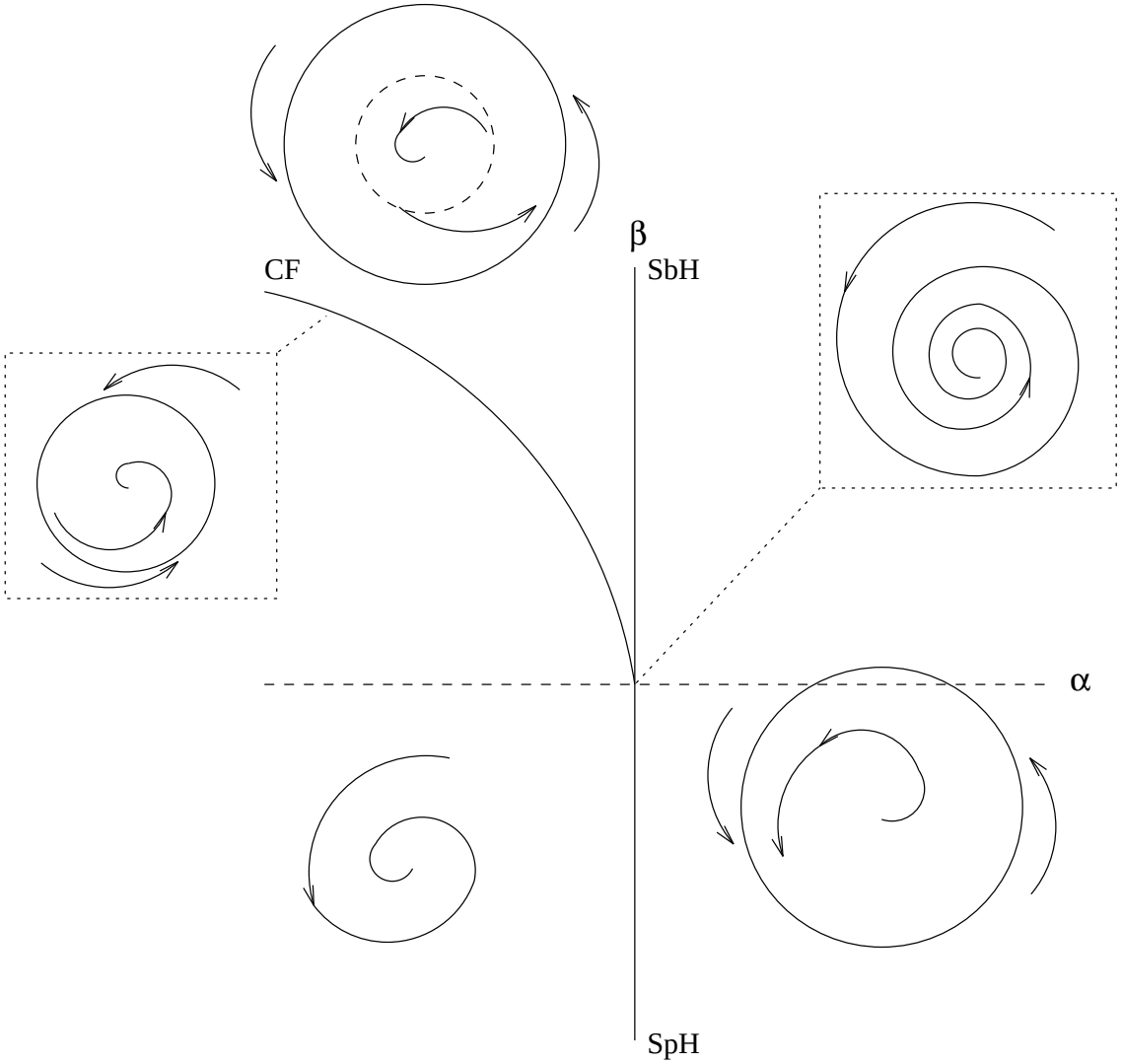

Two varities: the above and the above with time reversal. Both are seen in the *Xenopus* model.

Figure 3.11: Unfolding of the Degenerate Hopf Bifurcation on the Parameter Plane.

Hopf bifurcations is subcritical, whereas for $\beta > 0$, the line of Hopfs is supercritical. This fact is very useful since, when looking at the parameter plane, it is not always apparent whether the Hopf curve is subcritical or supercritical. To fully understand what is happening, let's move around the parameter plane (Fig. 3.11) counterclockwise. Starting in the third quadrant, the system has a single stable fixed point with no limit cycles. Crossing the supercritical Hopf bifurcation curve changes the stability of the fixed point and introduces a unique and stable limit cycle. This survives throughout the right half plane and as the curve of subcritical Hopf is crossed. Crossing the SbH curve creates an unstable limit cycle inside the stable limit cycle. Meanwhile, the fixed point regains its stability. Two limit cycles of opposite stability continue to exist until they are destroyed as they collide at the cyclic fold bifurcation curve. As we cross the CF curve, we are left with a stable fixed point.

Takens-Bogdanov : TB

At a Takens-Bogdanov bifurcation, we have a curve of SL bifurcations and a curve of Hopf bifurcation collapsing onto a curve of SN bifurcations. A normal form for the TB is

$$\dot{x} = y$$

$$\dot{y} = \alpha + \beta x + x^2 + xy.$$

A TB bifurcation, otherwise known as *double zero bifurcation*, has a nilpotent linearization. The equilibrium has a double zero eigenvalue and the trace of the Jacobian matrix is equal to zero. Moving clockwise around the parameter plane (Fig. 3.12), we see the following: starting in the right half plane, there are no fixed points (and no limit cycles). As we cross over the lower SN bifurcation curve it creates two fixed points–a saddle and a node. The node turns into a focus and loses stability as we cross the Hopf bifurcation curve. Also a stable limit cycle is born. As we cross the SL bifurcation curve, the limit cycle becomes homoclinic to the saddle point and is thereby destroyed by a saddle-loop bifurcation. As one traces the SL towards the TB, the loop-like orbit shrinks and disappears. Above the SL curve there are no cycles, but an unstable node and saddle exist. These two fixed points collide and disappear as we cross over the saddle-node curve, above the TB bifurcation, and return to the right half plane. At the TB, the critical fixed point with a double zero eigenvalue has exactly two asymptotic orbits. One converges to the fixed point and the other diverges from it. These orbits form a peculiar "cuspoidal edge" (e.g. [15]).

Neutral Saddle-Loop : NSL

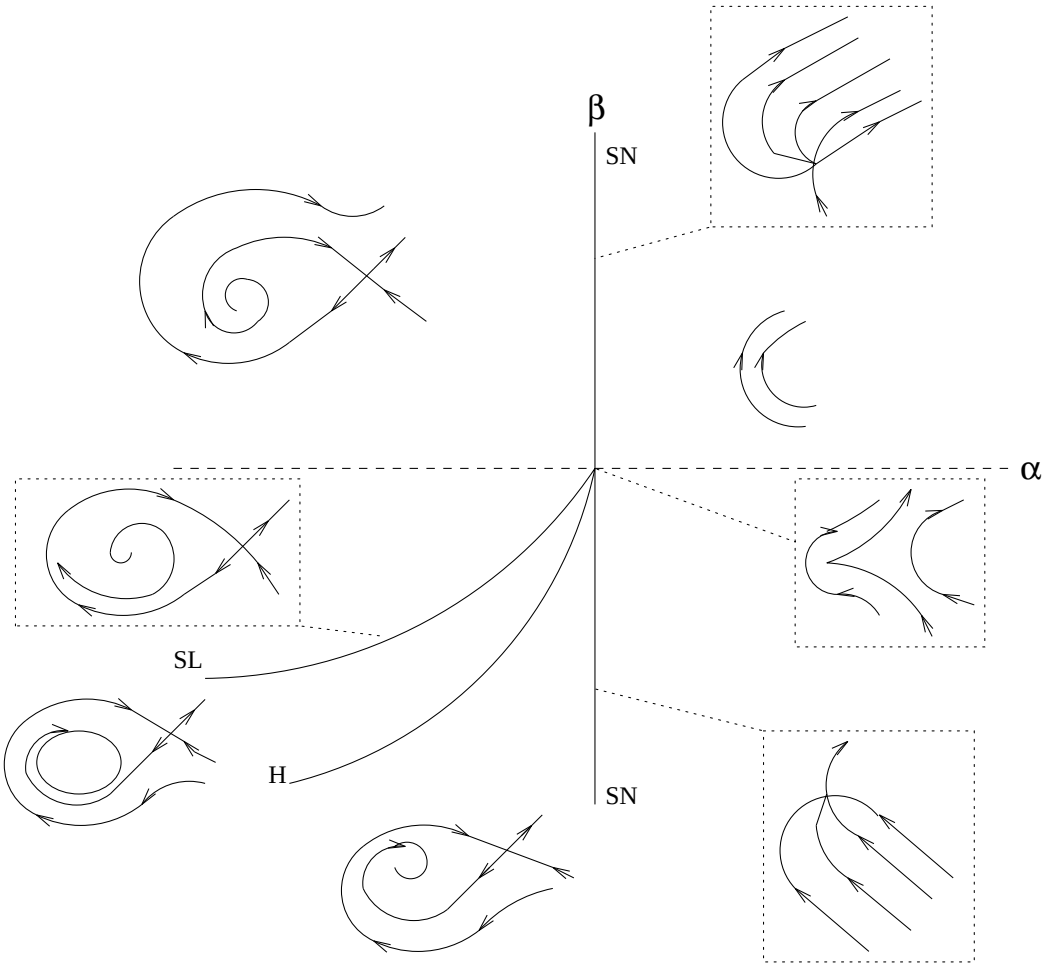

Two varieties: the one pictured above and the above with time reversal which is seen in the *Xenopus* model.

Figure 3.12: Unfolding of the Takens-Bogdanov on the Parameter Plane.

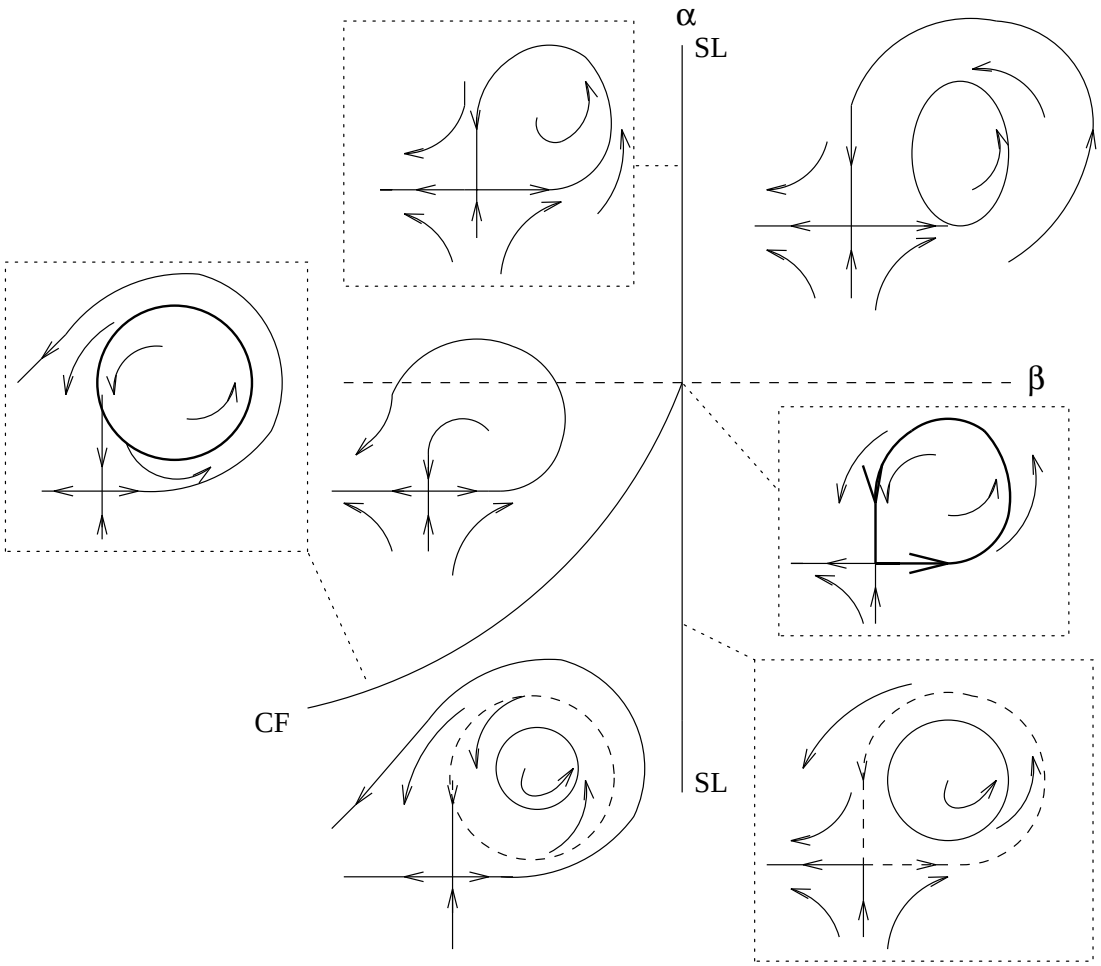

Two varieties depending on the stability of the nodes. The above and the above with time reversal. Both are seen in the *Xenopus* model.

Figure 3.13: Unfolding of the Neutral Saddle-Loop Bifurcation on the Parameter Plane.

Several dynamical changes are happening at a neutral saddle-loop bifurcation, also called *trace-zero saddle-loop*. First, as can be seen in the unfolding (Fig. 3.13), a curve of cyclic folds ends at a curve of saddle loops. The CF curve approaches the curve of SL tangentially with infinite order contact. The second dynamical change is that the infinite periodic orbits, represented by the SL curve, change their stability at the NSL bifurcation.

For two dimensional systems, the stability of nearby periodic orbits is determined by the trace of the Jacobian matrix at the saddle point. The trace of the Jacobian matrix equal to zero, implies that the periodic orbits are changing stability. Therefore we get the name trace zero or neutral saddle-loop. In higher dimensional systems the stability is still dependent on only two eigenvalues: in general those closest to the imaginary axis. See discussion of saddle loop bifurcation for the structure of the eigenvalue we have in the *Xenopus* model.

Moving counter clockwise around the parameter plane (Fig. 3.13), we see the following: in the right half of the plane we have a saddle point and a stable limit cycle. As we cross the upper SL curve, we lose the stable limit cycle leaving only a saddle point. As we move down the left half plane, we cross the cyclic fold curve where a stable and unstable limit cycle are born. These both continue until the lower SL curve is crossed and the unstable limit cycle is destroyed. This puts us back in the right half plane where we again have a stable limit cycle and a saddle point. As we move from left to right through the NSL bifurcation, we have a neutral limit cycle being destroyed via a saddle-loop bifurcation. As we move from the top half of the plane down through the NSL bifurcation, we have the limit cycle that is homoclinic to the saddle changing stability.

Saddle-Node-Loop : SNL

The phase portrait of the SNL bifurcation could be confused with the phase portrait of the codimension-1 SNIC bifurcation. However, there is one fundamental difference. The orbit of the SNL forms a closed curve or separatrix in the boundary of the invariant manifold. Guckenhiemer, in [17] described SNLs in the following way. “More precisely, assume that an equilibrium of a two-dimensional vector field has one negative and one zero eigenvalue and that the quadratic expression appearing in the saddle-node normal form is non-zero. For such a saddle-node, there is a half-plane of trajectories tending towards the equilibrium and a single unstable separatrix leaving it. The separatrix of the equilibrium (its unstable manifold) can have three distinct behaviors:

1. It can form a closed curve lying in the interior of the stable manifold
2. It can form a closed curve lying in the boundary of the stable manifold

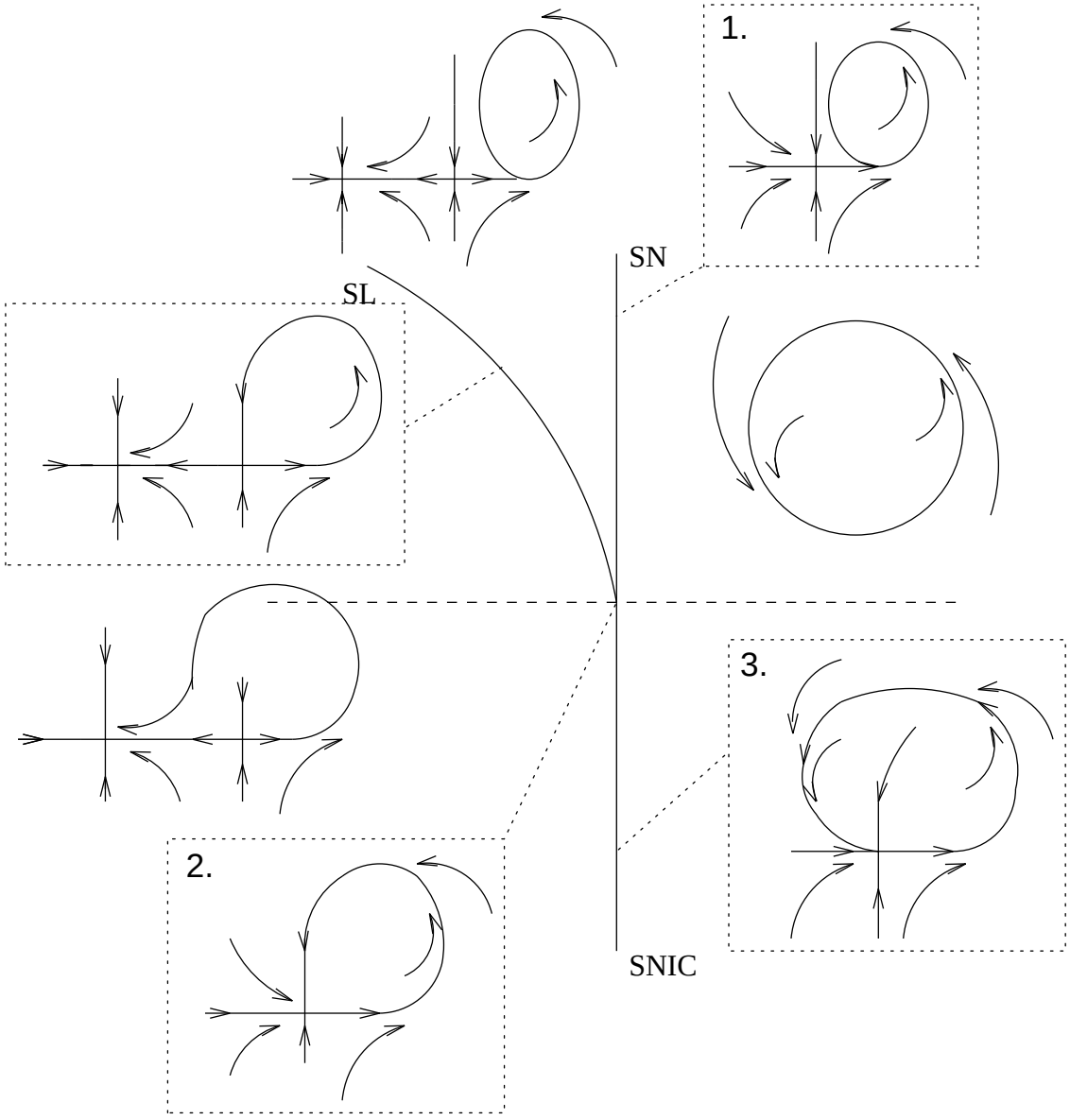

Four varieties depending on the stability of the nodes: (s,x,u)-pictured above, (s,x,s), (u,x,s), and (u,x,u). First and second are seen in the *Xenopus* model. Second two are simply the first two with time reversed (s=stable node, x=saddle, u=unstable node).

Figure 3.14: Unfolding of the Saddle-Node-Loop Bifurcation on the Parameter Plane.

3. It can lie outside the stable manifold.

The second behavior characterizes the saddle-node-loop" (see labels in Fig. 3.14). See also [18].

Moving counter clockwise around the parameter plane (Fig. 3.14), we see the following: in the right half plane we have a stable limit cycle with no fixed points. As we move through the SN curve, two fixed points are born–a saddle and a node. As we cross the SL curve, the limit cycle is destroyed and we are left with the saddle and node. As we cross the SNIC bifurcation curve, a limit cycle is born and a SN bifurcation takes place which destroys the saddle and node. At the SNL bifurcation, we have a closed curve lying in the boundary of the stable manifold.

Chapter 4

Bifurcations of Xenopus Model

In this chapter I will describe the two parameter bifurcation diagram of the *Xenopus* model. Fig. 4.1 summarizes the results of my numerical investigation. Because the diagram is very complicated, I will look at individual pieces of the diagram in great detail. In order to get a feel for the structure of trajectories, I will present phase portraits of the different regions in the parameter plane. One parameter bifurcation diagrams will also prove useful in describing the behavior of the system.

The parameters chosen are the Rate Constant for Cyclin Synthesis (**RCCycS**) , k_1 in mathematical model on page 11, and the Rate Constant for Cyclin Degradation (**RCCycD**), $V_{2''}$. The importance of cyclin synthesis in the activation of MPF, leading to the events of mitosis, was seen in chapter 2. Cyclin degradation is necessary to exit mitosis and begin a new division cycle. In order to see the interplay of these two rate constants, I chose **RCCycD** for a second parameter to vary. By studying the bifurcation diagrams, we will see how small changes in these parameters can have dramatic effects on the dynamics of the mathematical model.

4.1 Two Parameter Bifurcation Diagram - Overview

The complete two parameter bifurcation diagram for the *Xenopus* model (Fig. 4.1) is best understood by looking first at the two main curves of saddle-nodes (Fig. 4.2). These curves meet at a cusp to form a wedge in the parameter plane. The saddle-node curves organize the fixed points and break the parameter plane into two regions. Inside the wedge there are three fixed points and outside the wedge there is only one. We will consider fixed

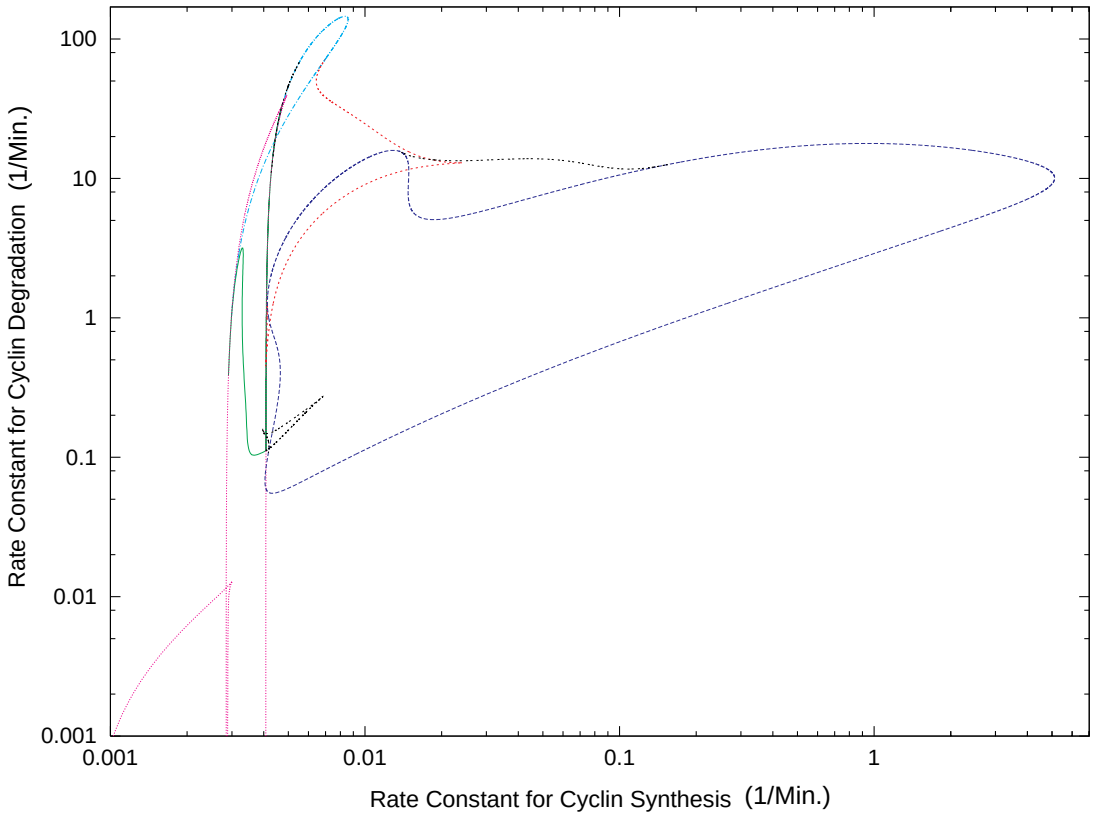

Figure 4.1: Two Parameter Bifurcation Diagram of the *Xenopus* Model– Overview.

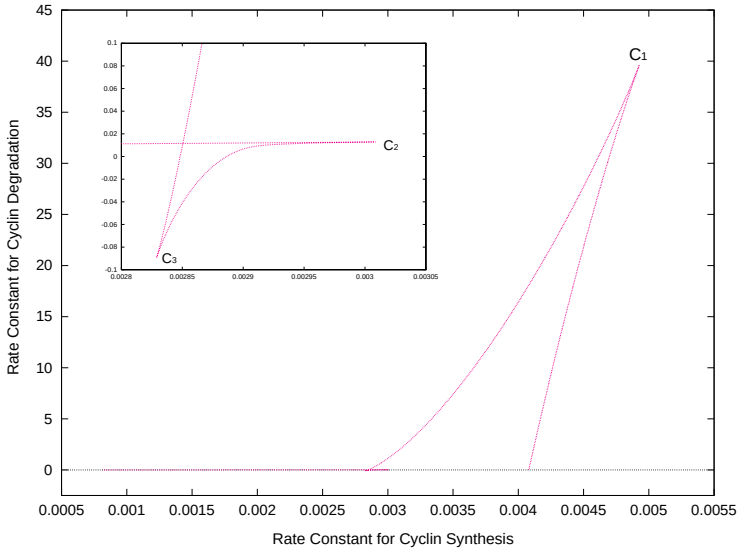

Sadde-node curves with cusp bifurcations. The three cusp bifurcations are located at (0.003,0.015), (0.0028,0.09), and (0.0049,39.6).

Figure 4.2: Two Parameter Bifurcation Diagram of the *Xenopus* Model.

points and limit cycles, and their stability in greater detail in the next section. Looking at the inlay of Fig. 4.2, we see that we have two more cusp bifurcations which give a small region having 5 steady states. Part of this region contains negative values for **RCCycD**. This region is irrelevant for the biochemical model, but I include it for completeness of the bifurcation diagram. Also at **RCCycS**=0.0028 and 0.0048 the left and right curves of saddle-nodes, respectively, become and stay negative for **RCCycD**.

On each of the main branches of saddle-nodes we have a Takens Bogdanov bifurcation, $\mathbf{TB_1}$ at (0.0029,0.384) and $\mathbf{TB_2}$ at (0.004353, 14.67), from which a curve of Hopf bifurcations begin and end (Fig. 4.3). Two saddle-loop bifurcation curves also begin at the TB bifurcations. The SL curve that begins at $\mathbf{TB_1}$ ends at $\mathbf{SNL_1}$ and the SL curve that begins at $\mathbf{TB_2}$ ends at $\mathbf{SNL_4}$ (see Fig. 4.4). There is also another SL curve that begins at $\mathbf{SNL_2}$ and ends at $\mathbf{SNL_3}$. Between $\mathbf{SNL_1}$ and $\mathbf{SNL_2}$, and $\mathbf{SNL_3}$ and $\mathbf{SNL_4}$ (Fig. 4.4), the infinite period orbits continue but are homoclinic to saddle-nodes and therefore are SNIC bifurcations. The stability of the homoclinic orbits is determined by the position of the neutral saddle-loop bifurcations. At $\mathbf{TB_1}$ (Fig. 4.4) the SLs are unstable and continue until $\mathbf{NSL_1}$ is reached where they become stable. We will shortly see the curve of cyclic folds that begins at $\mathbf{NSL_1}$ (Fig. 4.8). The saddle-loops become SNIC bifurcations at $\mathbf{SNL_1}$ but then become SLs again as the SNICs are destroyed and a new curve of SLs is born at $\mathbf{SNL_2}$. The homoclinic orbits that have remained stable since $\mathbf{NSL_1}$ become unstable at $\mathbf{NSL_2}$

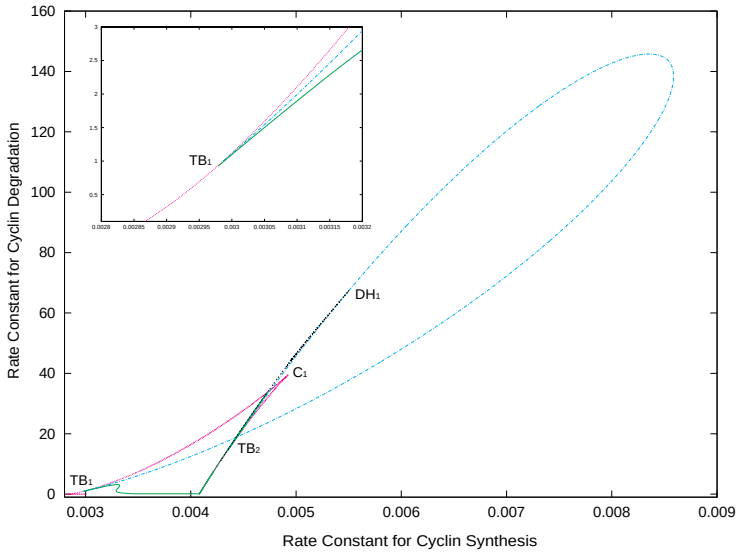

Added to Fig. 4.2 is a curve of Hopf bifurcations, a curve of cyclic folds, and several curves of saddle-loops and SNIC bifurcations. Emanating from both Takens Bogdanov bifurcations is a curve of Hopfs and saddle-loops.

Figure 4.3: Two Parameter Bifurcation Diagram of the *Xenopus* Model.

where we also see a curve of cyclic folds emanating from this point. The unstable SLs are destroyed at $\mathbf{SNL_3}$ where a curve of unstable SNICs is born and then quickly destroyed at $\mathbf{SNL_4}$ where a final curve of unstable SLs is born and then, as already seen, destroyed at $\mathbf{TB_2}$. The curve of cyclic folds that was born at $\mathbf{NSL_2}$ is destroyed at a degenerate Hopf bifurcation as it meets the curve of Hopf bifurcations at $\mathbf{DH_1}$. See Fig. 4.4.

The second curve of Hopf bifurcations (Fig. 4.5) is independent of the rest of the diagram in the sense that it does not begin or end at a codimension-2 bifurcation, but rather forms a closed curve in the parameter plane. However, we will soon see that there are several cyclic folds which connect this curve to the rest of the diagram via degenerate Hopf bifurcations. Looking at Fig. 4.6, we see two degenerate Hopf bifurcations $\mathbf{DH_3}$ and $\mathbf{DH_4}$ where a curve of cyclic folds begins and ends. Another degenerate Hopf bifurcation $\mathbf{DH_5}$ is seen in Fig. 4.7 where a curve of cyclic folds begins and then, after several cusp bifurcations, ends as it joins the first curve of Hopfs at a degenerate Hopf bifurcation $\mathbf{DH_2}$. The final curve in our two parameter diagram is another curve of cyclic folds that, as already mentioned, emanates from $\mathbf{NSL_1}$ and then after several cusp bifurcations ends at our final degenerate Hopf $\mathbf{DH_6}$. See Fig. 4.8.

Using Fig. 4.9 we will consider the nature of the curves of Hopfs, in particular, whether they are subcritical or supercritical. Below $\mathbf{DH_6}$ the curve of Hopfs is supercritical and

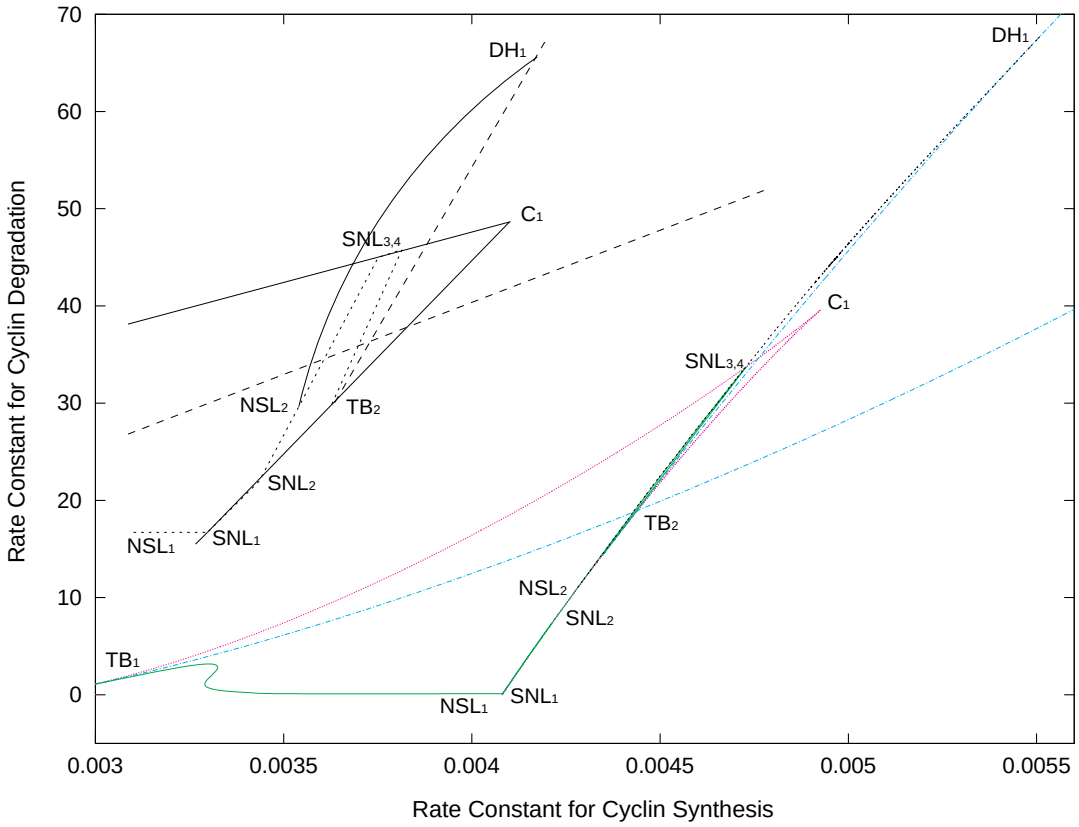

Closer look at Fig. 4.3. Because certain regions are so small, I give a sketch of the curves (upper portion of graph) that is not to scale.

Figure 4.4: Two Parameter Bifurcation Diagram of the *Xenopus* Model.

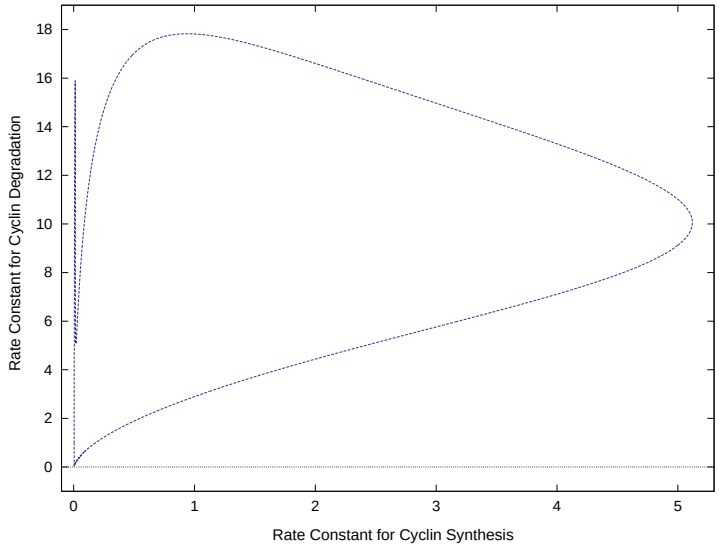

Second curve of Hopf bifurcations. Behavior of the curve for **RCCycS** close to zero can be seen in Fig. 4.6, Fig. 4.7, and Fig. 4.8.

Figure 4.5: Two Parameter Bifurcation Diagram of the *Xenopus* Model.

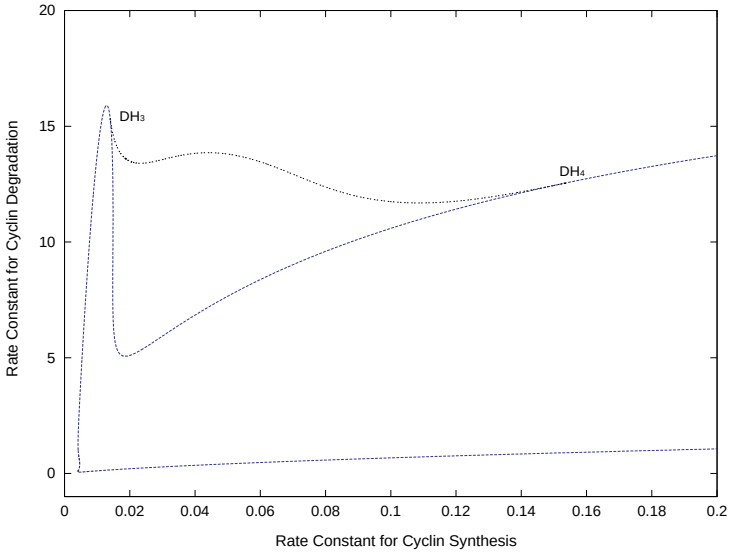

Hopf curve (Fig. 4.5) with cyclic fold curve connected by degenerate Hopf bifurcation.

Figure 4.6: Two Parameter Bifurcation Diagram of the *Xenopus* Model.

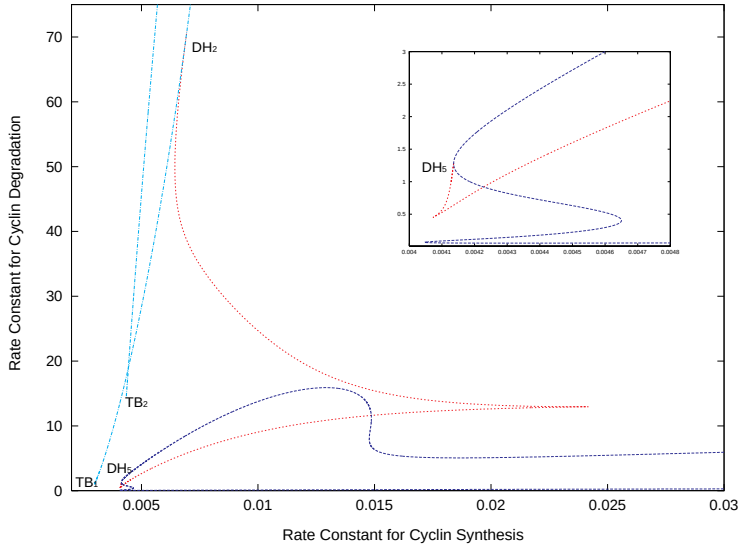

Both Hopf curves and several curves of cyclic folds which are joined to each other by cusp bifurcations and to the Hopf curves by degenerate Hopf bifurcations.

Figure 4.7: Two Parameter Bifurcation Diagram of the *Xenopus* Model.

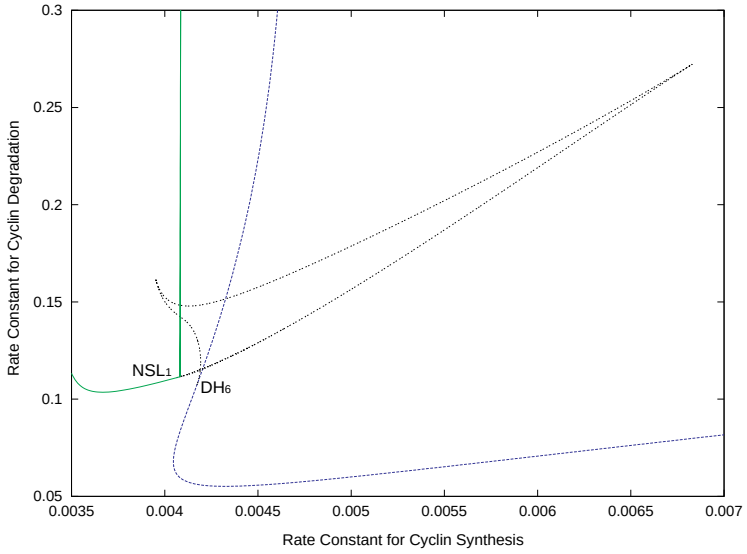

Bottom left corner of Hopf curve (Fig. 4.5). Final curves of cyclic folds joined to each other by several cusp bifurcations, to the curve of Hopfs by a degenerate Hopf bifurcation, and to the saddle-loop curve by a neutral saddle-loop bifurcation.

Figure 4.8: Two Parameter Bifurcation Diagram of the *Xenopus* Model.

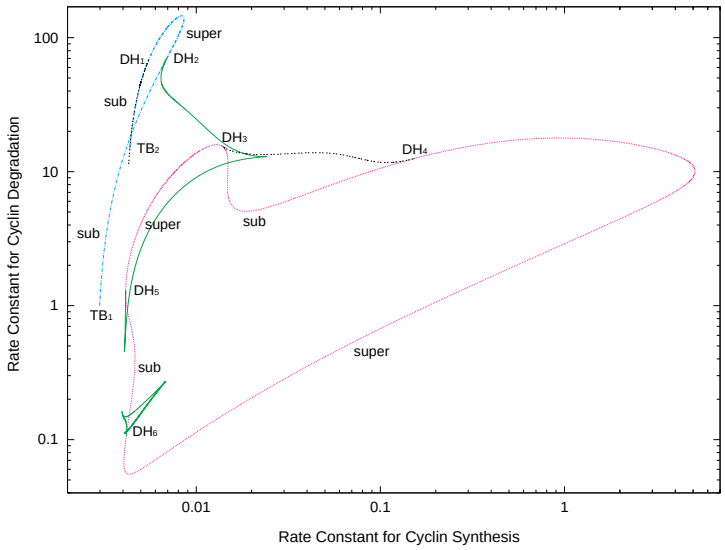

Two Hopf curves and all the curves of cyclic folds that are in the *Xenopus* model. Where these curves meet at degenerate Hopf bifurcations, the Hopf curve changes from supercritical to subcritical or vice versa.

Figure 4.9: Two Parameter Bifurcation Diagram of the *Xenopus* Model.

remains that way as we follow it down, around, and back up to $\mathbf{DH_4}$ where it changes to subcritical. In between $\mathbf{DH_4}$ and $\mathbf{DH_3}$ the curve of Hopfs continues to be subcritical but changes back to supercritical at $\mathbf{DH_3}$. In between $\mathbf{DH_3}$ and $\mathbf{DH_5}$ we have supercritical Hopfs which change to subcritical at $\mathbf{DH_5}$. They remain subcritical until a final change is made back to supercritical as we arrive back at $\mathbf{DH_6}$. Considering the first curve of Hopfs, at $\mathbf{TB_1}$ the Hopf bifurcations are subcritical and remain that way until $\mathbf{DH_2}$ is reached, at which point they change to supercritical. In between $\mathbf{DH_2}$ and $\mathbf{DH_1}$, the Hopfs are supercritical but change back to subcritical at $\mathbf{DH_1}$ and remain subcritical until the curve ends at $\mathbf{TB_2}$.

4.2 Two Parameter Bifurcation Diagram - Detailed Description

I will now describe the two parameter bifurcation diagram in greater detail by using phase portraits and one parameter bifurcation diagrams. This will serve the following purposes. First, it will show us what type of behavior we have in regions separated by codimension one bifurcation curves. Second, it will verify the completeness of the diagram. Finally, it

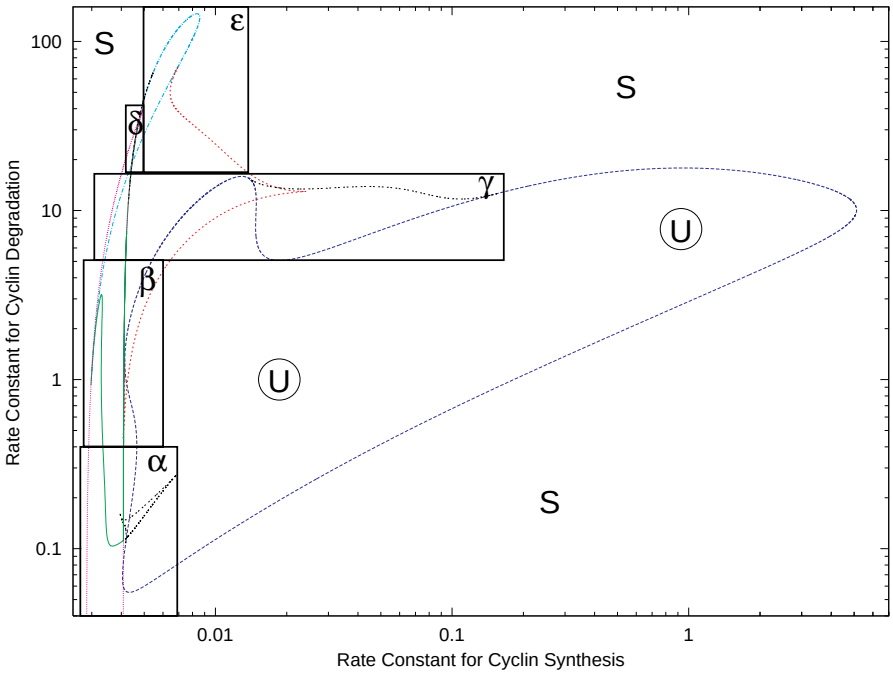

Two parameter bifurcation diagram. S=stable, U=unstable, X=saddle, and solid circles=stable limit cycles. We will look at the regions labeled with Greek letters in more detail: see Fig. 4.11 for a closer look at region α, Fig. 4.14 for β, Fig. 4.16 for γ, Fig. 4.19 for δ, and Fig. 4.21 for ϵ.

Figure 4.10: Key to Diagrams α - ϵ.

will give a better understanding of the dynamical behavior of the model, which we will need in order to draw conclusions (in the next chapter) about the biochemical model from the mathematical analysis. This description will not be comprehensive, in that I will not discuss in detail every region in the two parameter plane. However by discussing the more complex regions, as well as regions around each type of codimension-2 bifurcation, an understanding of the dynamics throughout should be achieved.

As already mentioned in the previous section, two main curves of saddle node bifurcations which meet at a cusp $\mathbf{C_1}$ (Fig. 4.2), organize the fixed points and break the parameter plane into two regions–inside the wedge there are three fixed points and outside the wedge there is only one. The two smaller curves of SN at **RCCycD** close to zero also give a region of three fixed points as well as a region of five fixed points (see bottom left of Fig. 4.11). As shown in Fig. 4.10, bordering the outside of the majority of the bifurcation diagram there is only one fixed point. Each of the eigenvalues corresponding to this fixed point is a negative real number, implying that the fixed point is a stable node.

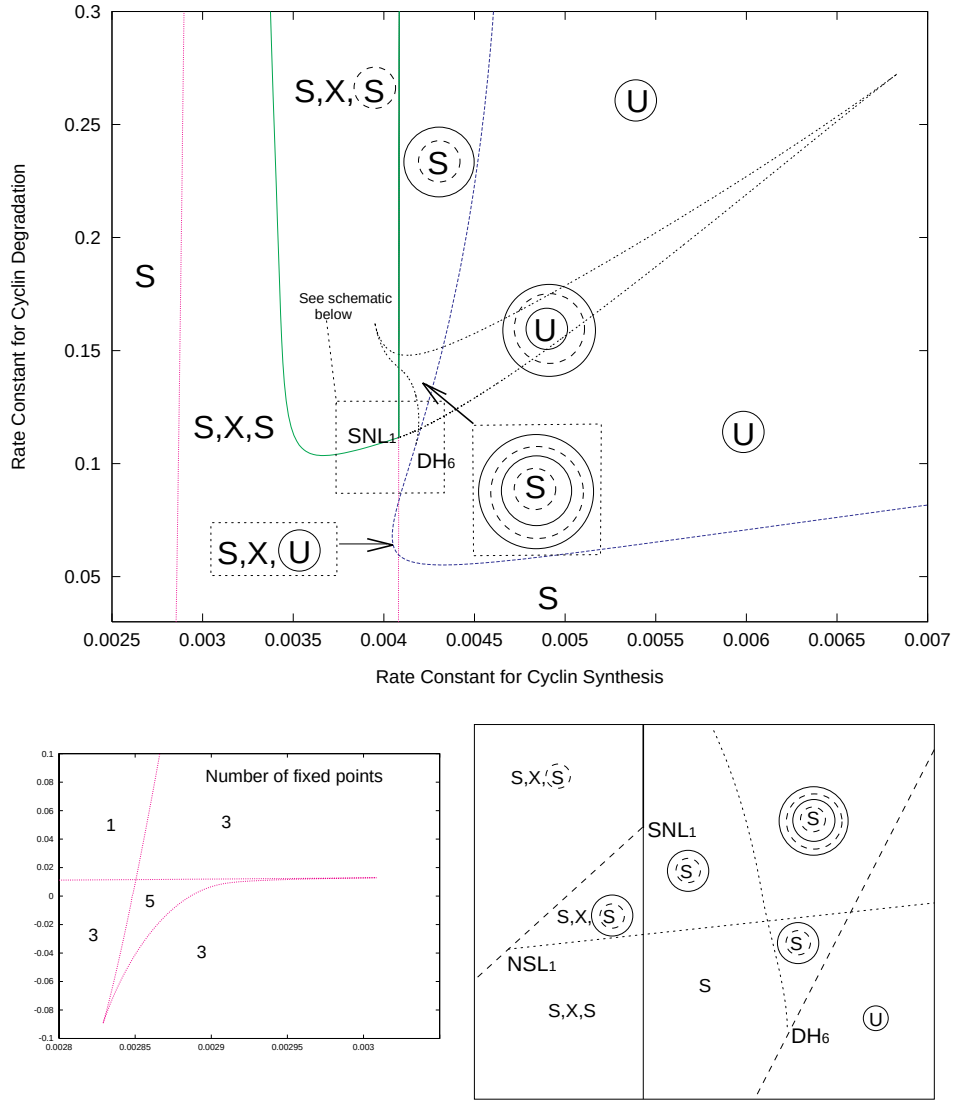

S=stable, U=unstable, X=saddle, solid circles=stable limit cycles, dashed circles=unstable limit cycles.

Figure 4.11: Region α.

Looking at Fig. 4.11 (region α of Fig. 4.10), let us start at **RCCycD**=0.25 and **RCCycS**=0.0025. As **RCCycS** increases, the SN curve is crossed which produces two new steady states–a saddle and a second stable node. Then as the saddle loop curve is crossed, an unstable limit cycle is born around the second stable node. Continuing on, we cross the second saddle node curve (which is actually a SNIC curve) where the initial node and saddle point coalesce and are destroyed. Also, a stable limit cycle is born around the unstable limit cycle which still surrounds the remaining node. Finally, we cross a Hopf curve where the unstable limit cycle disappears and the node becomes unstable. There are several curves of cyclic folds. Crossing a CF fold curve either produces a stable and unstable limit cycle or destroys them, depending on the direction that the curve is crossed. How the Hopf, CF, SL, and SNIC curves interact to create or destroy limit cycles can best be seen in a one parameter bifurcation diagram (Fig. 4.12). Also see Fig. 4.13 for the phase plane of the SNIC bifurcation in this region.

Before moving on to the next region let us look in detail at the dynamics around the codimension-2 bifurcations. Because they are so close and certain regions cannot be discerned, I have drawn a schematic diagram (in the lower right of Fig. 4.11). Moving counterclockwise around the $\mathbf{NSL_1}$, the following is observed: below the curve of cyclic folds (dotted) there is a saddle, two stable nodes, and no limit cycles. As the CF curve is crossed, a stable and unstable limit cycle are born around the second stable node. The stable limit cycle is destroyed as it becomes homoclinic to the saddle point at a stable saddle loop (dashed). This leaves only the unstable limit cycle and the fixed points on the upper side of the SL curve. The unstable limit cycle is destroyed as the SL curve is crossed to the left of the $\mathbf{NSL_1}$. Notice that the stablity of the homclinic orbits on the SL curve has changed at the neutral saddle-loop.

Moving counter clockwise around $\mathbf{SNL_1}$, we see the following: in between the SL and cyclic fold curves there is a saddle and two nodes of which the second is surrounded by an unstable limit cycle which is surrounded by a stable limit cycle. As the SN curve is crossed, the saddle and initial node are destroyed but the second node and limit cycles remain. Crossing back over the SN curve above the $\mathbf{SNL_1}$, a SNIC bifurcation is encountered. A saddle-node bifurcation takes place and the stable limit cycle is destroyed as it becomes homoclinic to the saddle-node. This leaves us with a saddle, two stable nodes, and an unstable limit cycle. As the curve of SL between $\mathbf{NSL_1}$and $\mathbf{SNL_1}$ is crossed, a stable limit cycle is born which surrounds the unstable limit cycle and the three fixed points remain as the region between the SL and cyclic fold curve is re-entered.

Now as we move into region β (Fig. 4.14), we see the same basic structure found in the top of region α except for one noticeable difference. At the Takens-Bogdanov bifurcation ($\mathbf{TB_1}$) we have a curve of Hopf and saddle-loops meet the curve of SN. As we move around this bifurcation, we see the following dynamics. To the left of $\mathbf{TB_1}$ we are outside the

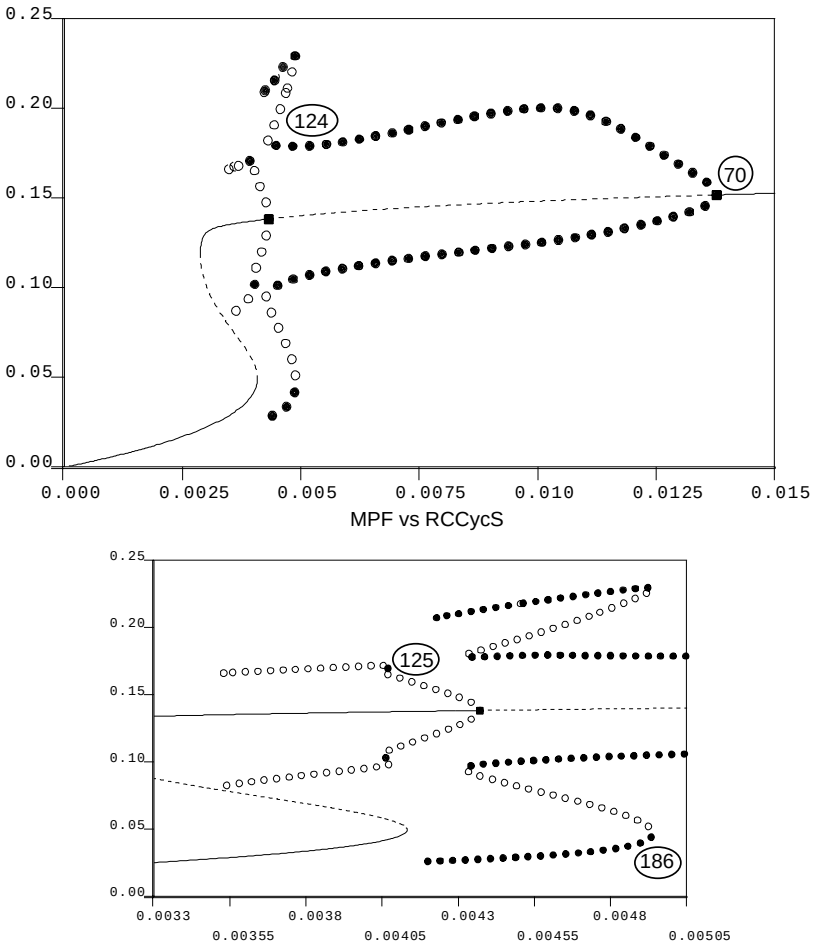

Solid lines=stable, dotted lines=unstable, filled circles=stable limit cycles, hollow circles=unstable limit cycles. Value in oval is period of nearby stable limit cycles. See Region α for comparison.

Figure 4.12: One Parameter Bifurcation Diagram with **RCCycD**=0.15.

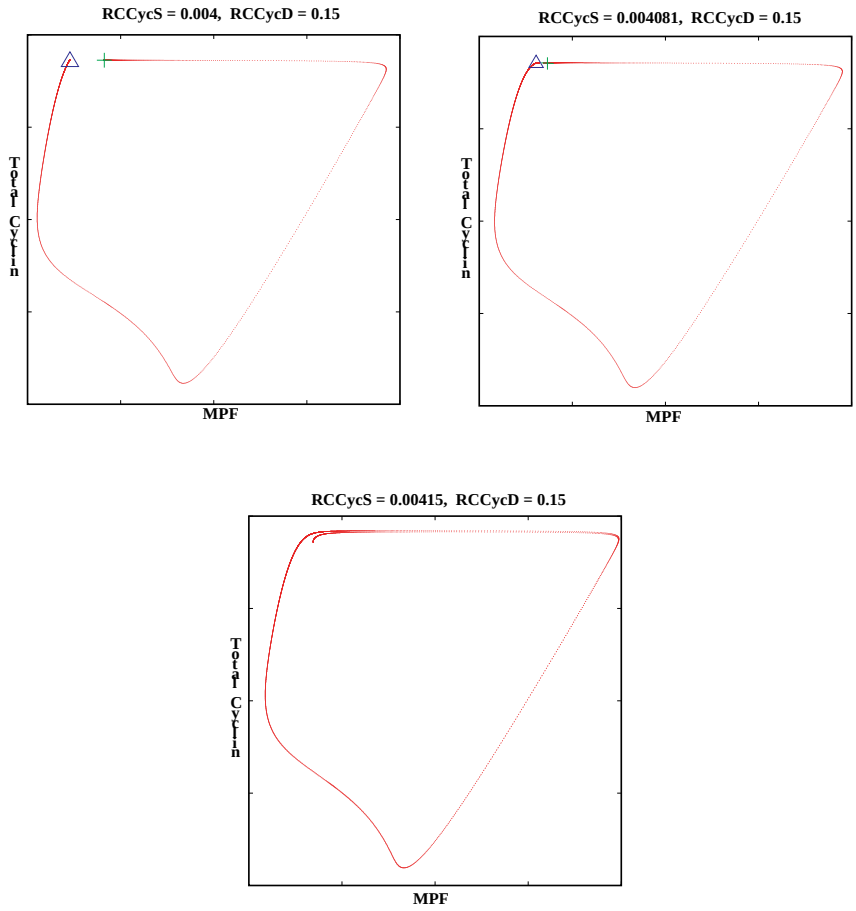

Triangle=node, cross=saddle. See Fig. 4.12 and Fig. 4.11 for one and two parameter bifurcation diagrams that include this SNIC.

Figure 4.13: SNIC Bifurcation for **RCCycD**=0.15 as **RCCycS** is varied.

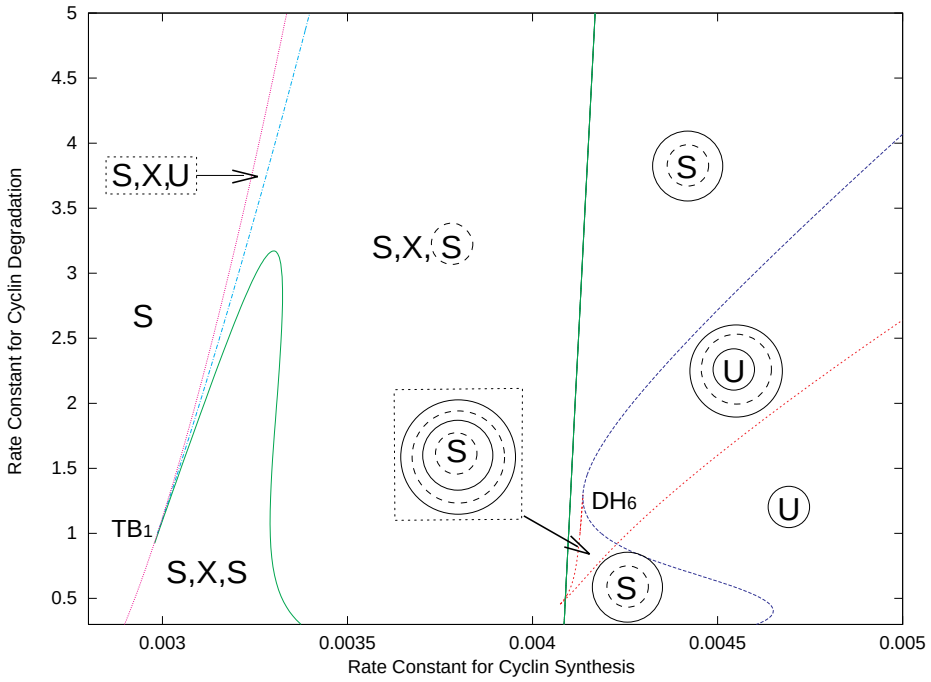

S=stable, U=unstable, X=saddle, solid circles=stable limit cycles, dashed circles=unstable limit cycles.

Figure 4.14: Region β.

wedge and have a stable steady state. As we cross the SN curve above $\mathbf{TB_1}$, a saddle and node are born. This is a different SN bifurcation than what we saw in Region α since the node that is born is unstable. As the curve of Hopfs is crossed, a subcritical Hopf bifurcation takes place. The unstable node becomes stable and an unstable limit cycle is born around it. This limit cycle is born with a high period (infinite at the $\mathbf{TB_1}$ and smaller as you move away) and is quickly destroyed as **RCCycS** is slightly increased and the curve of unstable SL bifurcation is crossed. In the region bounded by the SL curve we have no limit cycles and three steady states. As we cross the SN curve, the saddle and second node (now stable) collide and are destroyed. This leaves us with a stable node as we move back outside the wedge. One thing to note is how the $\mathbf{TB_1}$ breaks the SN curve up into a curve that creates a saddle and stable node and a curve that creates a saddle and unstable node. The SL curve seen in region β is before $\mathbf{NSL_1}$, and therefore it either produces or destroys an unstable orbit. The second line of SN at **RCCycS**=0.0041 is overlayed by the stable SNIC bifurcation curve from $\mathbf{SNL_1}$. As **RCCycS** is increased through this curve, a stable limit cycle is born which ends on the other side of our large curve of Hopfs (Fig. 4.10). See Fig. 4.15 for a one parameter cut across Region β for **RCCycD**=2.5. Also, to see how the qualitative behavior changes as **RCCycD** is increased above the arch of saddle-loops, compare lower graphs of Fig. 4.15.

I now go above to region γ (Fig. 4.16). This region is about three times larger for both **RCCycS** and **RCCycD**. A logrithmic scale is used for **RCCycS**. On the left branch of SN as well as within most of the wedge there is little change from the top of region β. However near the other SN branch we have several codimension-2 bifurcations surrounded by very small regions of different qualitative behavior. Because of this fact, I have drawn a schematic diagram (Fig. 4.23) that includes parts of regions γ and ϵ and all of region δ. I will discuss these small regions after the general behavior of the total diagram is reviewed. Understanding the part of region γ that is outside the wedge should be clear from our previous look at Hopf and cyclic fold curves in regions α and β. Because of the shape in this region of the large curve of Hopfs and the $\mathbf{TB_2}$, there are multiple Hopf bifurcations (four below $\mathbf{TB_2}$ and five above) as **RCCycD** is varied across the plane for fixed values of **RCCycD**. See Fig. 4.17. Also see Fig. 4.13 for the phase plane of the SL bifurcation in this region.

In Region δ (Fig. 4.19) we have very complex behavior in extremely small regions of parameter space. This entire region will be blown up in a schematic (Fig. 4.23) and so I will defer any discussion of it until then. See Fig. 4.20 for a one parameter bifurcation cut at **RCCycD**=30.

As we come to our last region (Fig. 4.21), there are several curves of cyclic folds that end on the Hopf bifurcation curve. The curve of CF that began at $\mathbf{NSL_2}$ is now ending at $\mathbf{DH_1}$, and the curve that began at $\mathbf{DH_5}$ is now ending at $\mathbf{DH_2}$. Above these degenerate

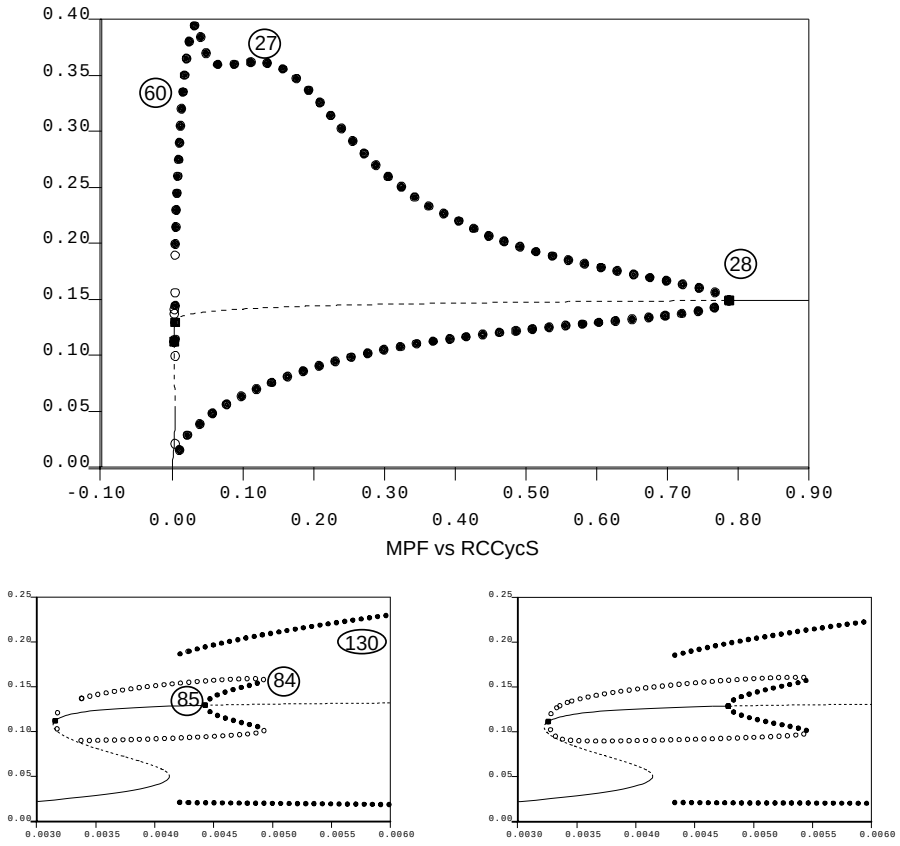

Solid lines=stable, dotted lines=unstable, filled circles=stable limit cycles, hollow circles=unstable limit cycles. Value in oval is period of nearby stable limit cycles. Lower right diagram is for **RCCycD**=3.5. Compare with lower left to see how behavior of the limit cycles changes as **RCCycD** decreases into region with double saddle loops. Also see Region β for comparison.

Figure 4.15: One Parameter Bifurcation Diagram with **RCCycD**=2.5 and (3.5).

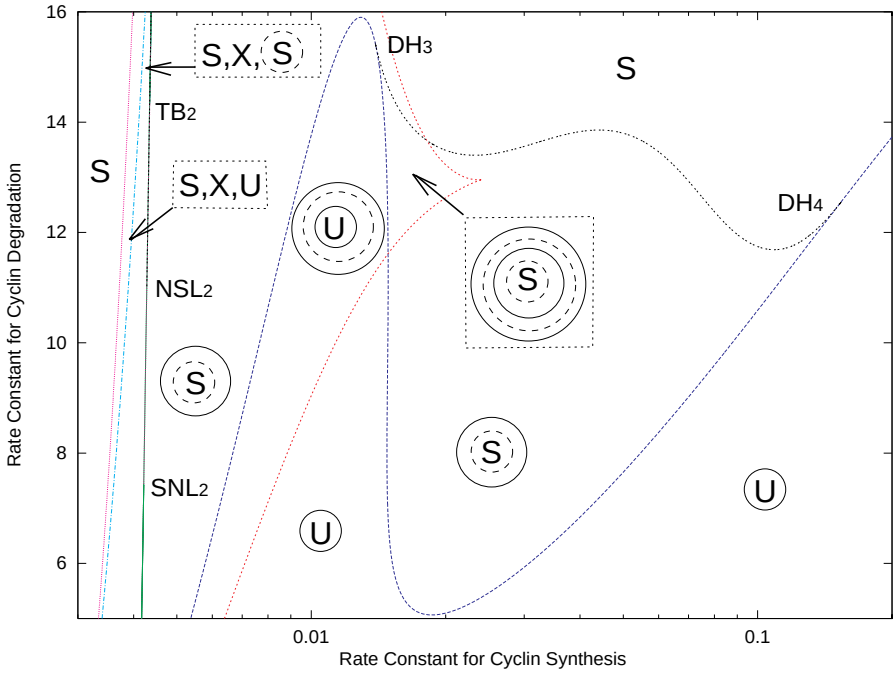

S=stable, U=unstable, X=saddle, solid circles=stable limit cycles, dashed circles=unstable limit cycles.

Figure 4.16: Region γ.

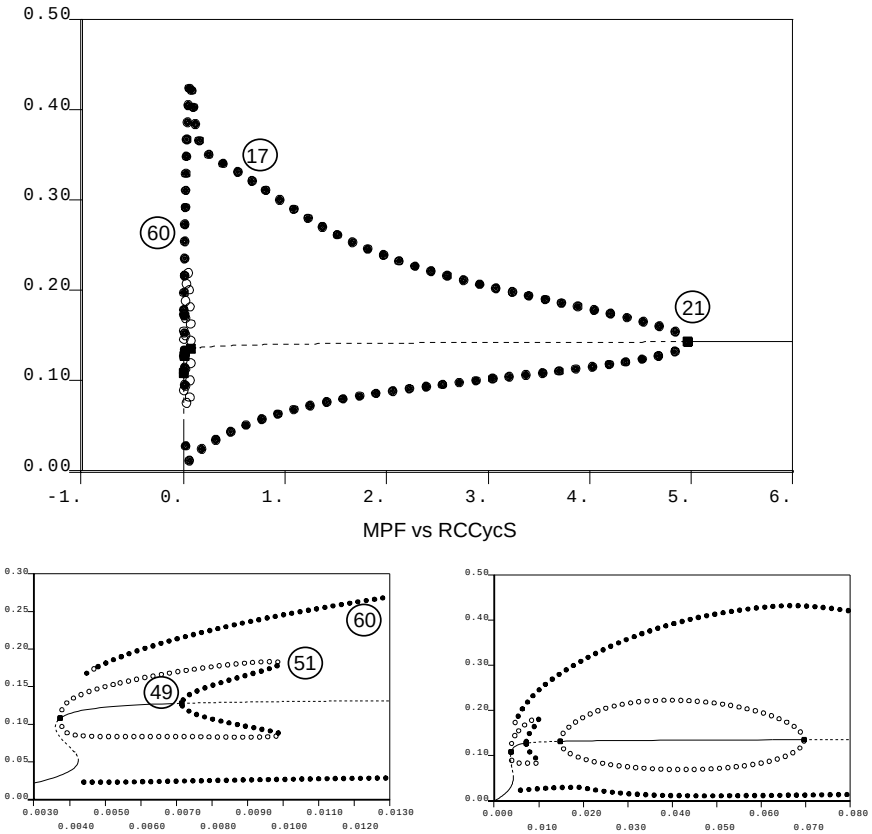

Solid lines=stable, dotted lines=unstable, filled circles=stable limit cycles, hollow circles=unstable limit cycles. Value in oval is period of nearby stable limit cycles (See Region γ for comparison).

Figure 4.17: One Parameter Bifurcation Diagram with **RCCycD**=9.0.

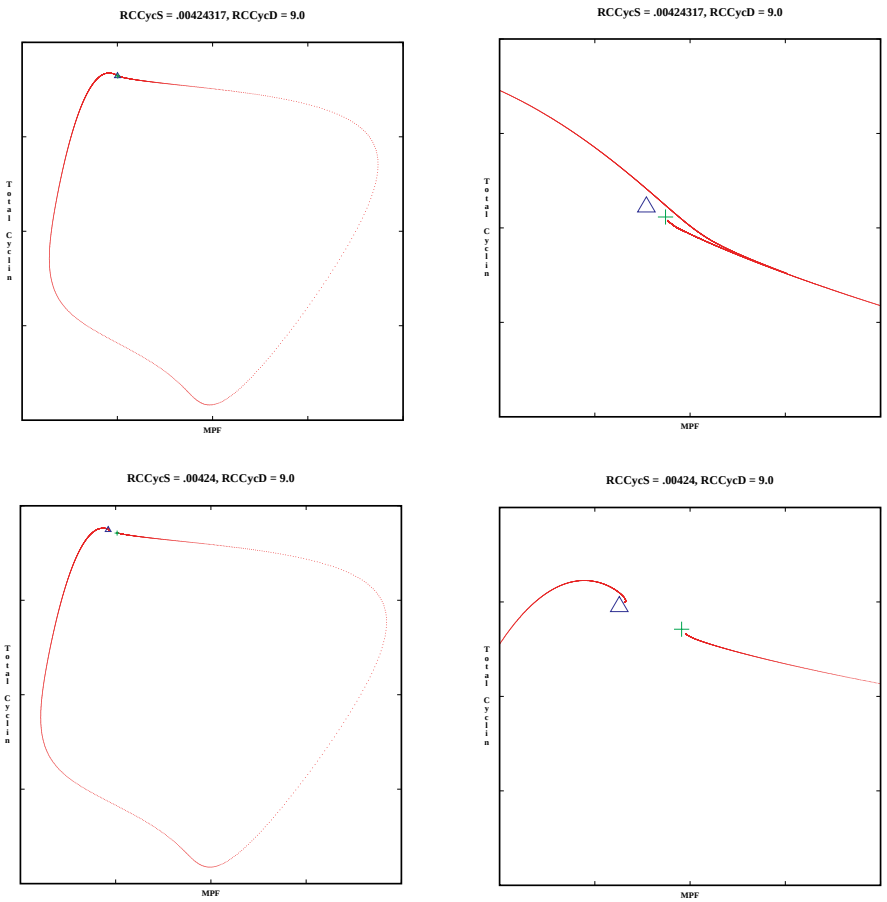

Triangle=node, cross=saddle. See Fig. 4.17 and Fig. 4.16 or Fig. 4.23 for one and two parameter bifurcation diagrams that include this SL.

Figure 4.18: SL Bifurcation for **RCCycD**=9.0 as **RCCycS** is varied.

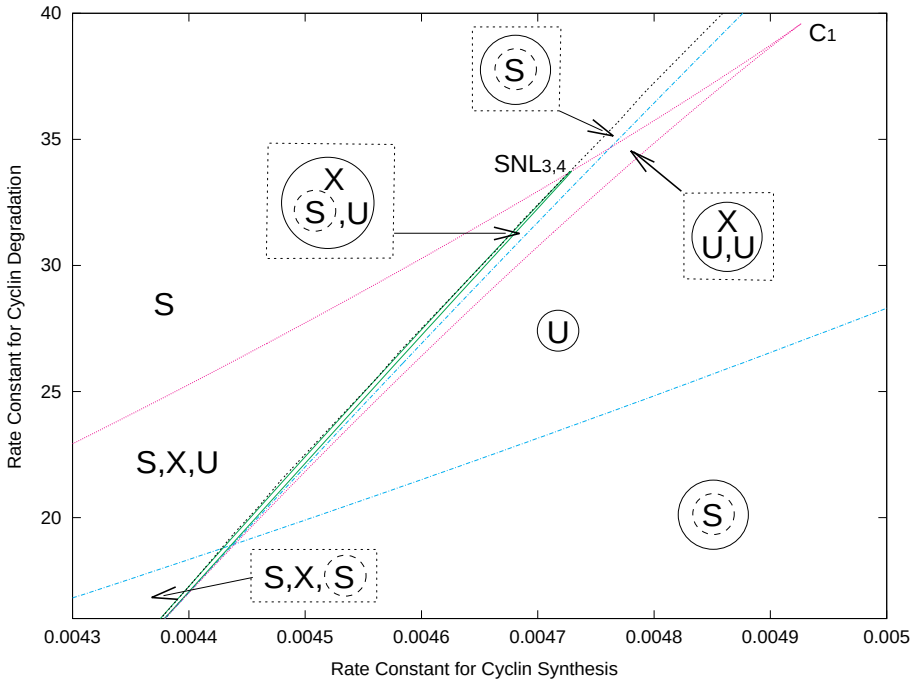

S=stable, U=unstable, X=saddle, solid circles=stable limit cycles, dashed circles=unstable limit cycles.

Figure 4.19: Region δ.

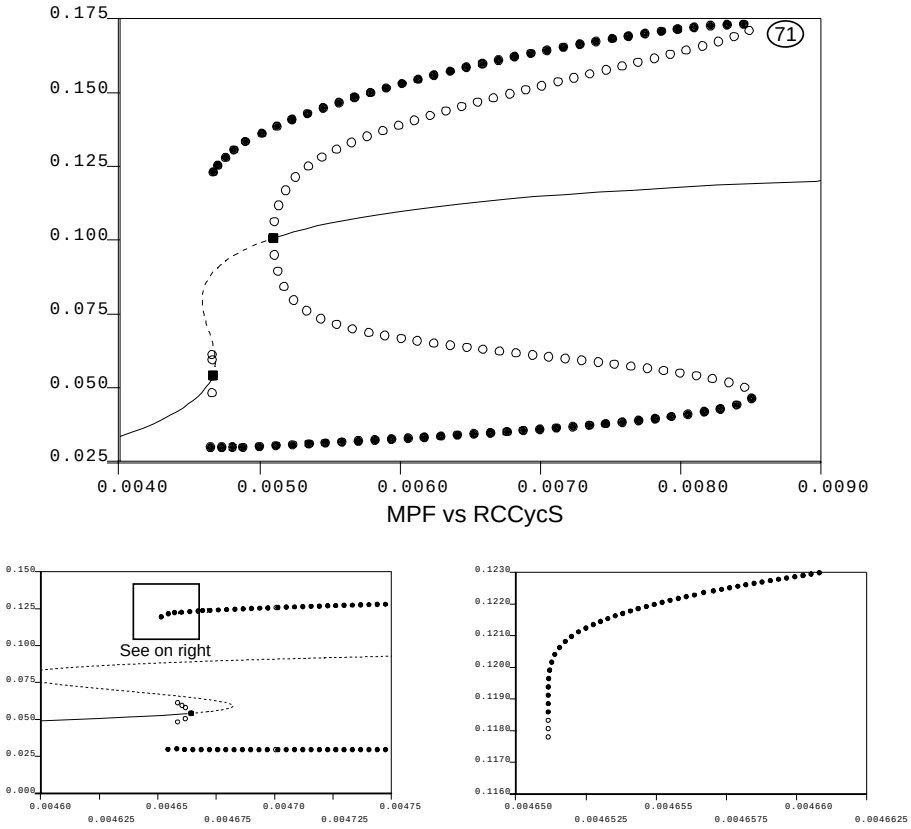

Solid lines=stable, dotted lines =unstable, Filled circles=stable limit cycles, hollow circles=unstable limit cycles. Value in oval is period of nearby stable limit cycles. Notice how the saddle-node bifurcations have come much closer together as the cusp $\mathbf{C_1}$ is approached. See Region δ for comparison.

Figure 4.20: One Parameter Bifurcation Diagram with **RCCycD**=30.0.

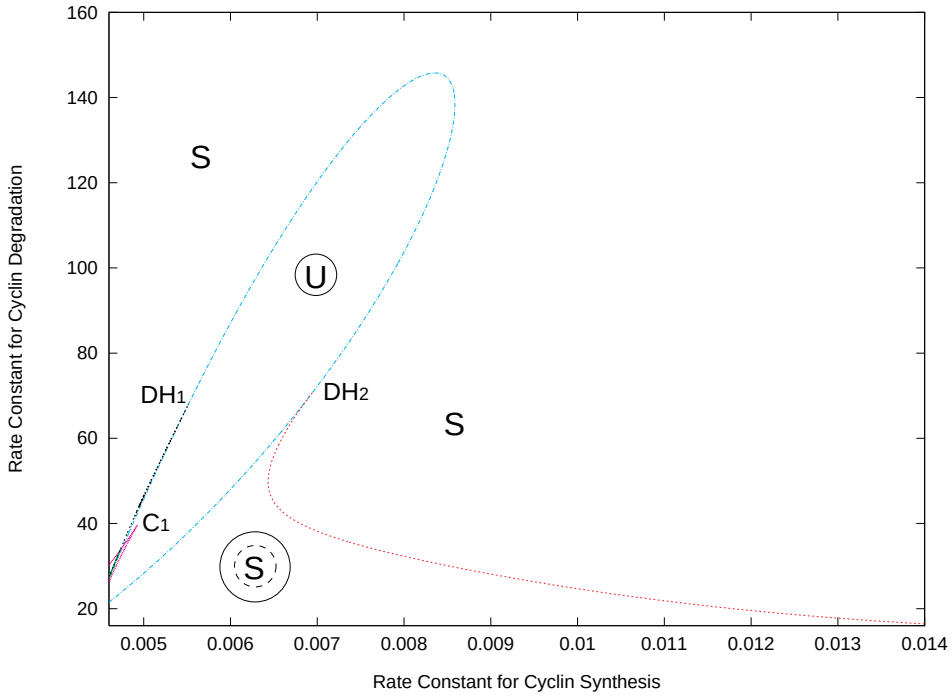

S=stable, U=unstable, solid circles=stable limit cycles, dashed circles=unstable limit cycles .

Figure 4.21: Region ϵ.

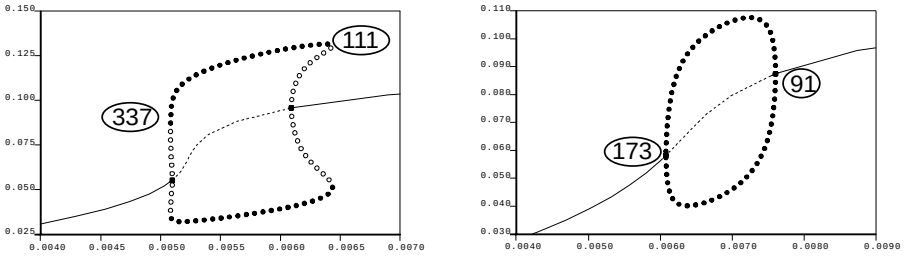

Solid lines=stable, dotted lines=unstable, filled circles=stable limit cycles, hollow circles=unstable limit cycles. Value in oval is period of nearby stable limit cycles.. (See Region ϵ for comparison)

Figure 4.22: One Parameter Bifurcation Diagram with **RCCycD**=50.0 and 90.0.

Hopf bifurcations, the curve of Hopfs is supercritical. So as we cross into this region a stable limit cycle is born around the now unstable steady state. These solutions continue down to the main cusp bifurcation $\mathbf{C_1}$. See Fig. 4.22 for one parameter bifurcation cut at **RCCycD**=50 and 90

Finally, using the schematic diagram (Fig. 4.23), let us move down from the cusp into the wedge. As we enter the wedge at $\mathbf{C_1}$, the 3 fixed points are very close and the stable limit cycle surrounds the saddle and both unstable nodes. Crossing either Hopf curve changes the stability of the respective node and introduces an unstable limit cycle. The unstable limit cycle that was begun by crossing the Hopf curve above $\mathbf{TB_2}$ is destroyed at the first saddle-loop curve between $\mathbf{SNL_4}$ and $\mathbf{TB_2}$. As the second curve of saddle-loops is crossed, an unstable limit cycle is born which surrounds all three fixed points. The large period stable and unstable limit cycles are destroyed as the curve of cyclic folds is crossed.

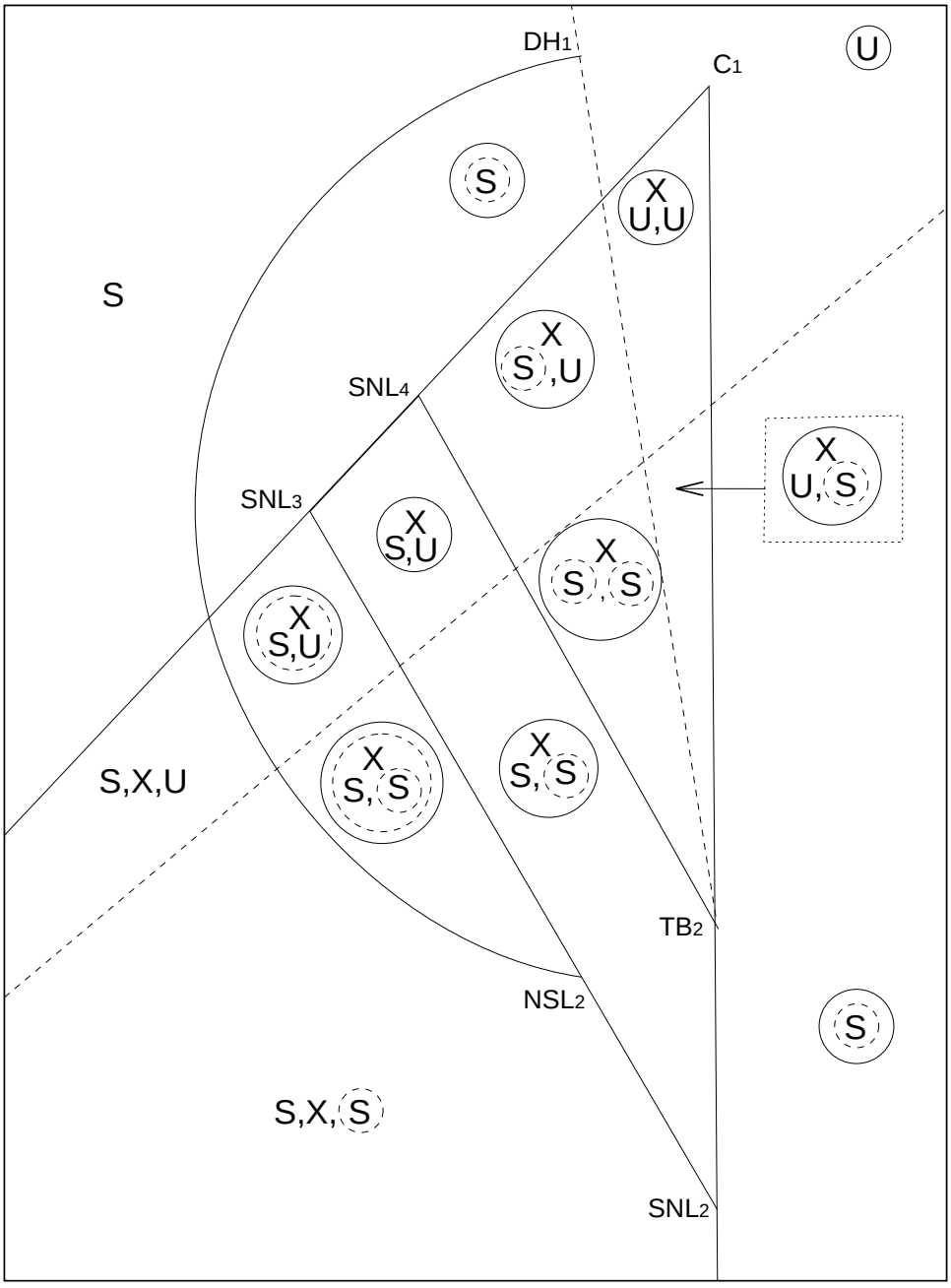

S=stable, U=unstable, X=Saddle, solid circles=stable limit cycles, dashed circles=unstable limit cycles.

Figure 4.23: Schematic Regions γ, δ, and ϵ.

Chapter 5

Bifurcations of the Biochemical Model

In this final chapter, I will use the information that has been extracted from the analysis of the mathematical model to make testable hypotheses of possible behavior in the cell cycle control system.

One cannot expect that every type of behavior seen in the mathematical model will be observable in frog egg extracts or that the numerical values of rate constants for which we see certain behavior are exact. Futhermore, I realize that this is a model that can and will be improved as the cell cycle contol system is better understood. This being said, Tyson and Novak [3] [19] have, with this mathematical model, simulated many of the most important experiments of frog egg extracts, proving the model to be qualitatively sound. Building on what they have already done, I will make several predictions of the behavior of frog egg extracts that can, in principle, be tested in the lab by molecular biologists. Also, even though the complexity of future models will most assuredly increase, the bifurcations and qualitative behavior that has been found in this model should carry over, to some extent, to models of greater complexity.

5.1 Biochemical results

I will first look at some results from the mathematical model of the frog egg cell cycle as described by Novak and Tyson [19]. Using phase portraits on a reduced system of equations, Novak and Tyson made several observations on the behavior of the mathematical model.

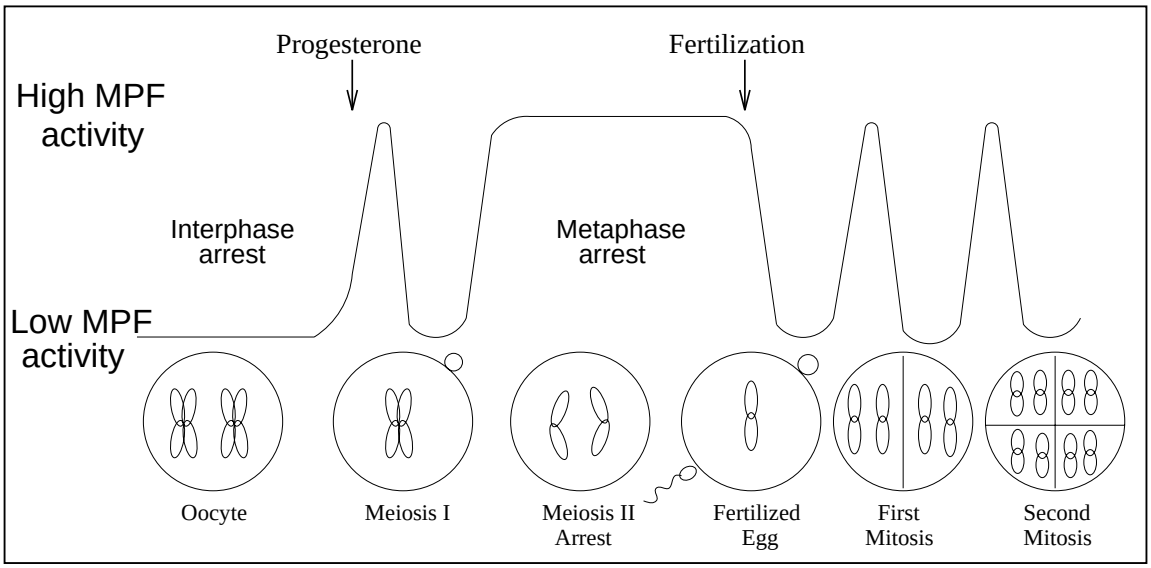

Oocytes have low MPF activity. Progesterone is added and induces the activation of MPF which leads to meiosis I. After a brief decline, MPF is activated again and the oocytes remain in metaphase arrest (meiosis II) with high levels of MPF. M-arrest is overcome by fertilization which leads to a decline in MPF activity, after which the mitotic oscillations of MPF are begun [1].

Figure 5.1: MPF Fluctuations in Meiotic and Mitotic Cell Cycles [1,Fig. 2-6].

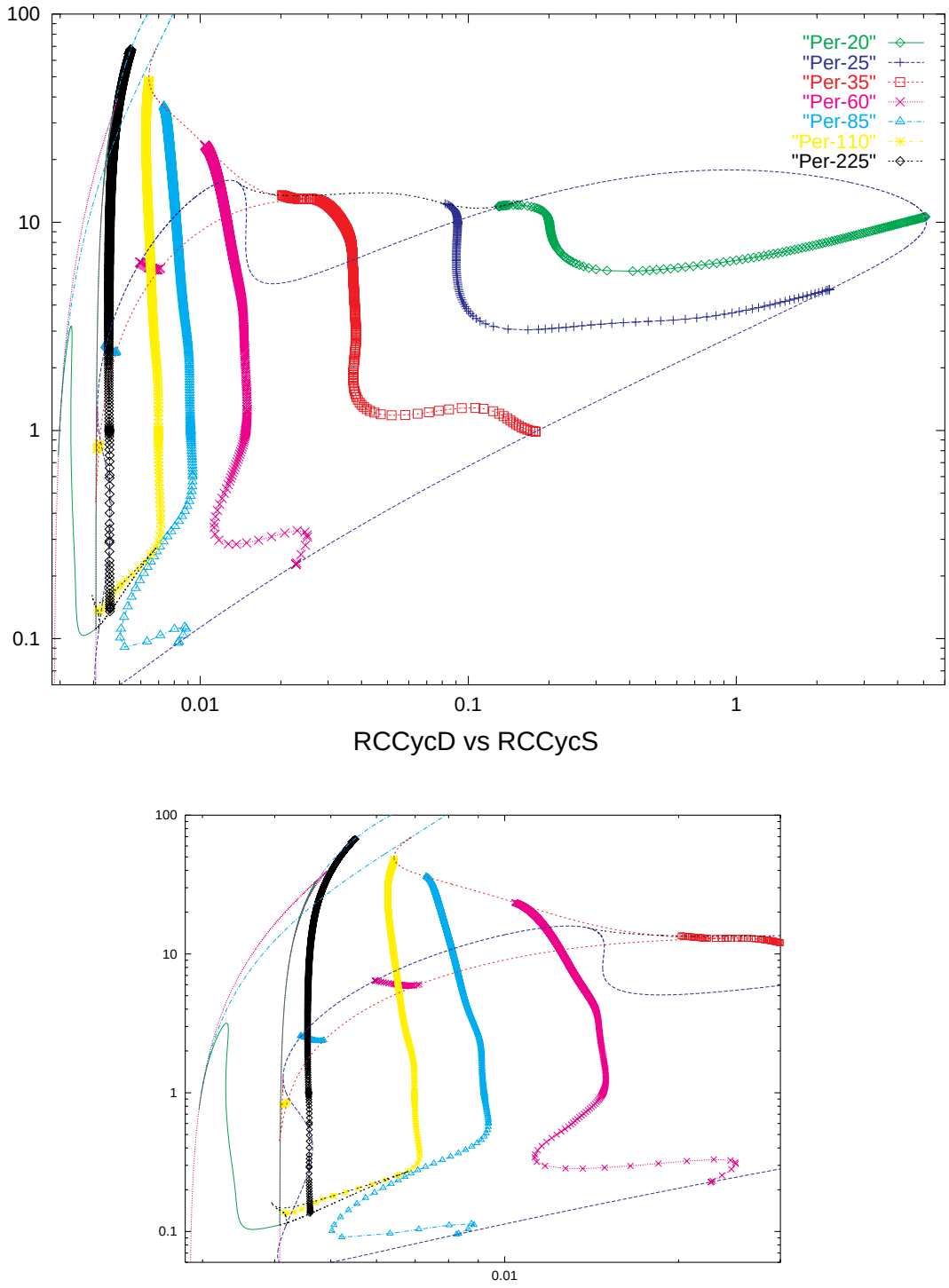

Figure 5.2: Stable Limit Cycles of period 20,25,35,60,85,110, and 225.

They found, for different parameter values, stable steady states with low MPF activity, stable steady states with high MPF activity, and unstable steady states surrounded by stable limit cycles. They also found a region with mulitiple steady states. These characteristic modes of behavior of the mathematical model can be associated with behavior that is seen in the frog egg: stable steady states with low MPF can be associated with interphase arrest (Fig. 5.1), stable steady states with high MPF activity with a metaphase arrested cell, and unstable steady states surrounded by stable limit cycles with the autonomous oscillations of MPF activity in early embryonic cell cycles. What bifurcations might connect these different modes was not addressed.

In chapters one and two, we saw the importance of cyclin synthesis as well as cyclin degradation on the control mechanism of the frog egg cell cycle. An equally important reason for choosing the rate constant for cyclin synthesis as a bifurcation parameter is the fact that it is relatively easy for experimentalists to manipulate in the laboratory by altering the amount of exogenous cyclin mRNA that is added to the extract. As I apply what was learned from the bifurcation analysis to the cell cycle, I will detail several possible experiments whose outcome is predicted from the mathematical analysis. This will not only give additional information on Novak and Tyson's model, but also give new insights into the mechanism of the cell cycle control system.

We first want to look at where in parameter space we have limit cycles with periods in the neighborhood of the 60 minutes that are seen in the frog egg extracts. Therefore, using AUTO [21], I followed in two parameters, limit cycles having certain periods. These are plotted in Fig. 5.2. The majority of the stable limit cycles with relatively small periods are in the region surrounded by the large curve of Hopf bifurcations. For large values of **RCCycS** we see that we have limit cycles with the smallest period and that these periods are insensitive to large fluctuations in **RCCycS**. As we get closer to the period of the oscillations that are seen in the frog egg extracts (60 minutes) we see that small fluctuations in **RCCycS** have large effects on the period of the stable limit cycles.

Where and how these limit cycles are created or destroyed is important in predicting experimental results. In Fig. 5.3, I have plotted all the bifurcation curves that begin or end stable limit cycles. As can be seen, there is a large region in the parameter plane with one stable limit cycle and also several smaller regions with two (these are the striped regions in Fig. 5.3). The lower of these regions close to $\mathbf{RCCycD} = 0.1$ is fairly small and the period of both limit cycles are quite large. However, the upper region is quite large and the period of both limit cycles is in the neighborhood of 60 for the majority of the region (see Fig. 5.2).

I will now detail some behavior predicted by the mathematical model and show how this prediction can be tested in the lab. I will pick $\mathbf{RCCycD} = 5.0$. There is a large interval

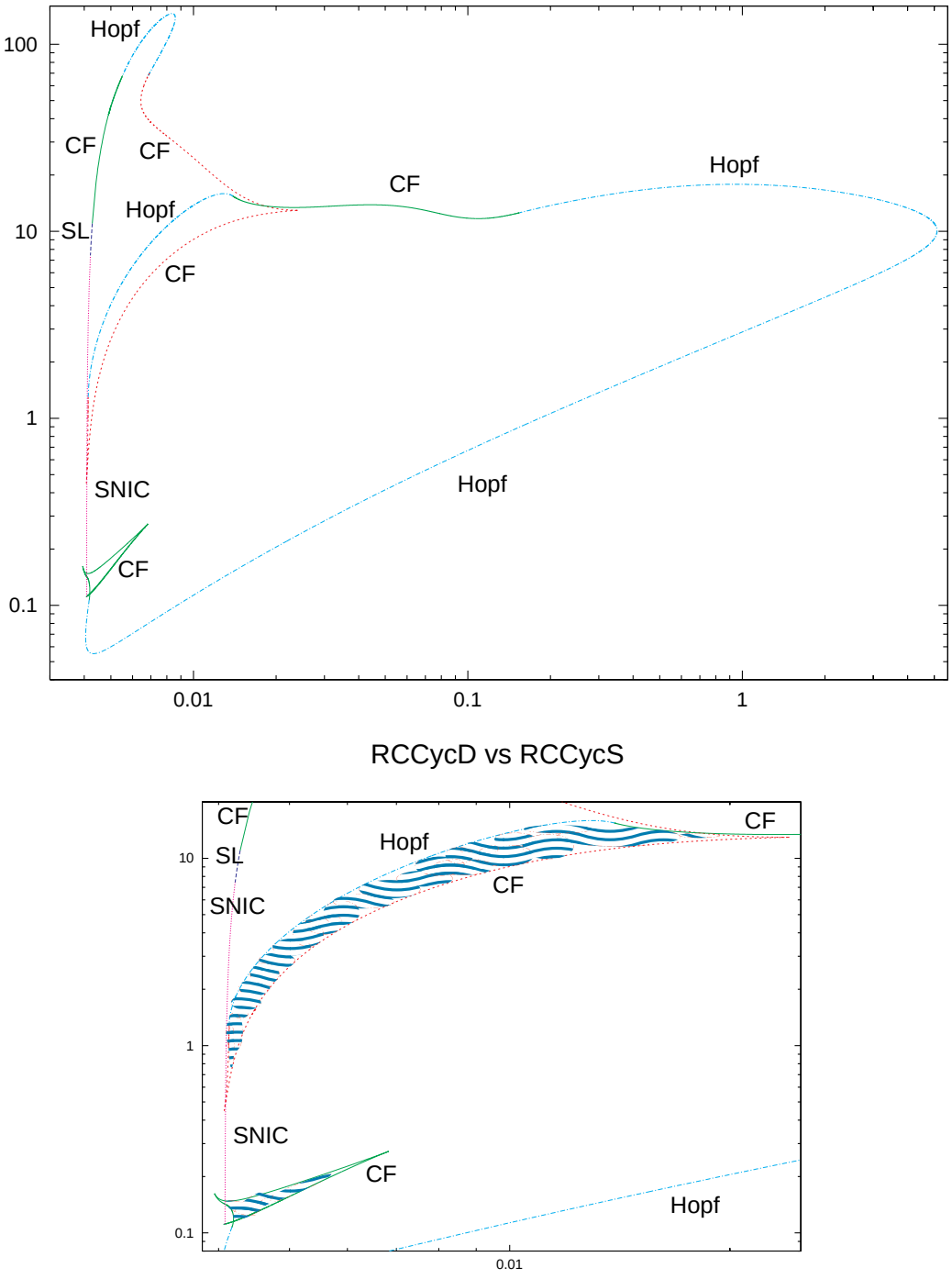

Figure 5.3: Creation and Destruction of Stable Limit Cycles.

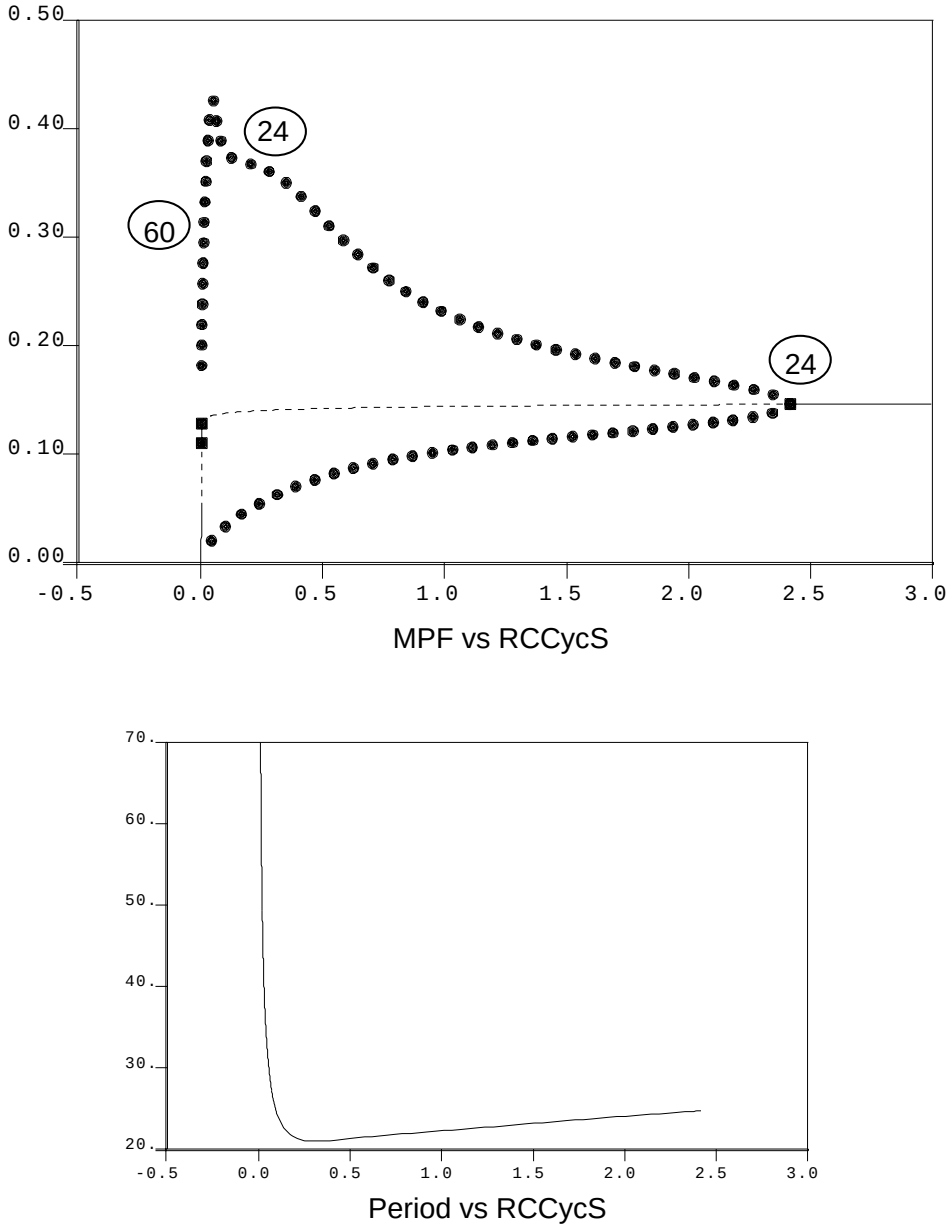

Figure 5.4: Qualitative Behavior as Cyclin mRNA is Increased.

around this value where the behavior that I will describe is predicted by the mathematical model. If we look at Fig. 5.4 we can see a one parameter diagram at **RCCycD**=5.0 as **RCCycS** varied. Labeled on the diagram are the periods of the limit cycles for different values of **RCCycS**. Starting at the limit cycles with period around 60 (**RCCycS**=0.01395) and increasing **RCCycS**, we can see (Fig. 5.4) the period of the limit cycles decrease rather sharply to begin with, but then remain fairly constant. The amplitude decreases to zero as the limit cycles are destroyed via a Hopf bifurcation. On the other side of the Hopf we have stable steady states with high MPF activity. Moving in the opposite direction from the limit cycles of period 60 (Fig. 5.5), we see that the limit cycles are not destroyed by a Hopf bifurcation, but in a completely different manner. As **RCCycS** is decreased the period increases rapidly. The amplitude, however, becomes constant as the period continues increasing to infinity, at which point the limit cycles are destroyed at a SNIC bifurcation (saddle loop bifurcation for larger values of **RCCycD**). We are left in a region with multiple steady states.

Once an egg extract is prepared, testing these predictions should be relatively easy. A small increase in the amount of cyclin messenger RNA (from the normal amount that produces the 60 minute cycles) should cause the period to decrease. The mathmatical model predicts that further increases should produce a drop in amplitude (the maximum and minimum values that MPF reaches will not be as large or as small, repectively), but that changes in period should remain fairly constant. Still further increases in mRNA should see oscillations with smaller amplitudes and steady periods until the amplitude of the oscillations go to zero. At this point the mathematical model predicts that the extract will reach a steady state (no oscillations) with high MPF activity.

If the amount of cyclin mRNA added is decreased (from that which produces 60 minute limit cycles), then the following behavior is predicted: for a relatively small decrease of mRNA, the amplitude will decrease and the period will increase. The decrease in the amplitude seems to be more in the maximum level of MPF coming down, whereas the minimum level remains somewhat fixed. For continued small decreases in mRNA, one should see that the amplitude becomes fixed and the period increases to infinity as the limit cycles are destroyed. When these oscillations cease we enter a region of three steady states. A stable state with low MPF activity, a saddle point, and stable or unstable steady state with high MPF activity. The extract will come to rest at one of the steady states. Because the limit cycles become homoclinic to the saddle-node that produces the steady state with low MPF, the extracts will come to rest with low MPF activity.

We will now move on and look at another region. If we hold **RCCycD**=9.0 and vary **RCCycS**, then we still have the same basic behavior as the region described above. In addition, there are several other things happening that are worth noting. Fig. 5.6 shows that we have a region of stable steady states surrounded by unstable limit cycles. Surrounding

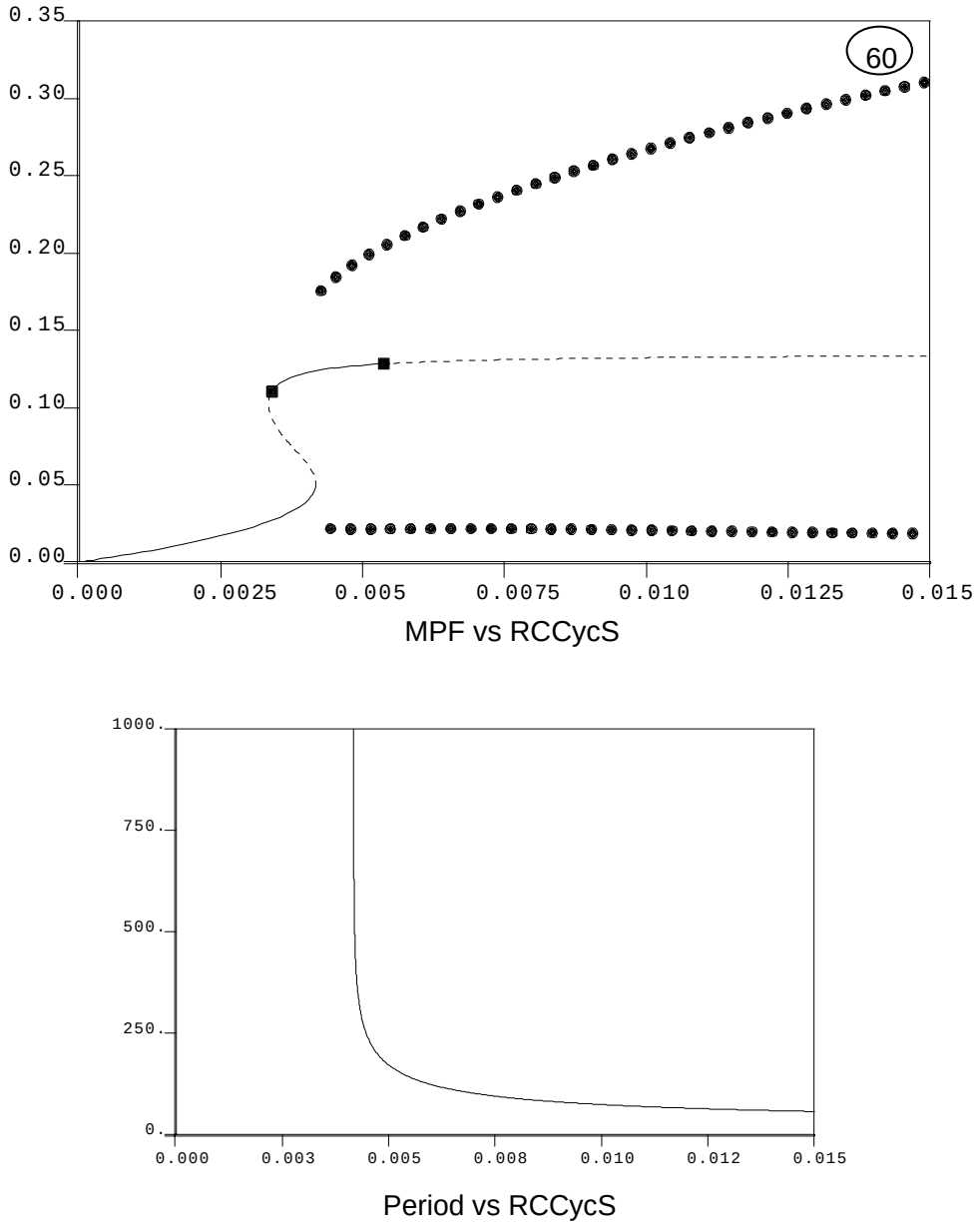

Figure 5.5: Qualitative Behavior as Cyclin mRNA is Decreased.

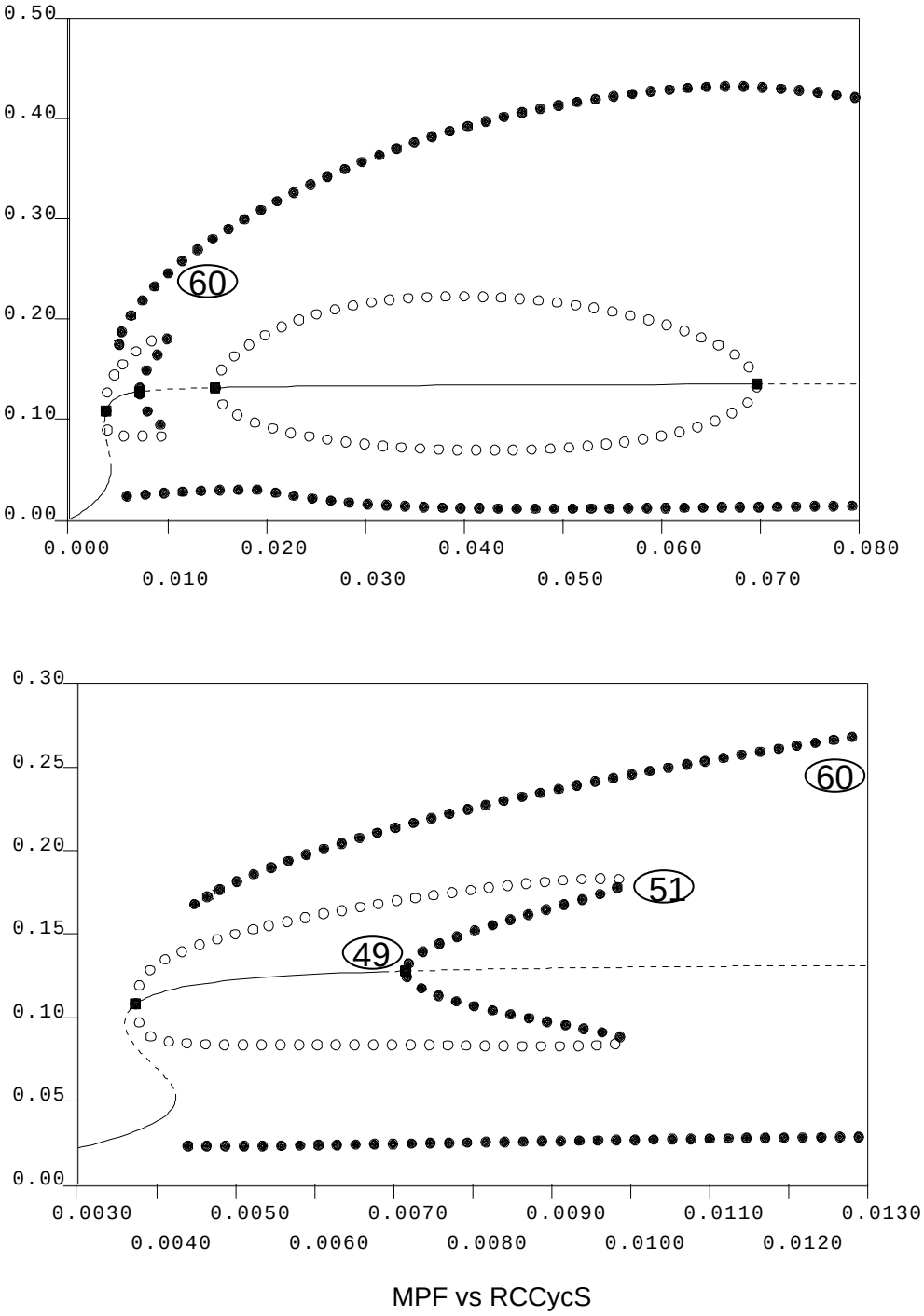

Figure 5.6: Bistability in the MPF Control System of Frog Eggs.

this entire region is the stable limit cycles similar to what we saw in Fig. 5.4. What makes this region worth noting is the following: for a fixed value of **RCCycS** we have two stable solutions–a stable steady state with high MPF activity and a stable limit cycle with period in the neighborhood of 60 minutes. This region could correspond to metaphase arrest in the cell (Fig. 5.1). During M-arrest, the cell has a high levels of MPF. M-arrest is overcome by fertilization, which leads to a precipitous decline in MPF activity. A decline in MPF could bring the solution "below" the minimum MPF of the unstable limit cycles. The solution would then be drawn to the stable limit cycles causing oscillations like the ones seen during mitosis. Experimental tests for this type of phenomenon would be the following: once the extract is in the equivalent of metaphase arrest, by artificially increasing MPF activity by a small amount, one should see MPF activity return to the steady state. However, a large change in MPF activity should produce oscillations of the type seen during mitosis.

Finally, as I have already noted, there is a fairly large region with two stable limit cycles (Fig. 5.3). These stable limit cycles can be seen in Fig. 5.6. In principle the coexistence of two stable limit cycles can also be demonstrated by perturbing the limit cycles with pulses of MPF, although this case would be considerably harder to prove experimentally.

Bibliography

[1] Andrew Murray and Tim Hunt, **The Cell Cycle**, Oxford University Press, 1993.

[2] B. Alberts, D. Bray, J. Lewis, M. Raff, K. Roberts, J. Watson, **Molecular Biology of the Cell**, Garland Publishing, Inc., New York, 1983.

[3] Bela Novak and John Tyson, *Numerical analysis of a comprehensive model of M-phase control in Xenopus oocyte extracts and intact embryos*, **Journal of Cell Science 106**, pp 1153-1168, 1993.

[4] Leah Edelstein-Keshet, **Mathematical Models in Biology**, McGraw-Hill, Inc., New York 1988.

[5] M.J. Solomon, M. Glotzer, T.H. Lee, M.Philippe and M.W. Kirschner, *Cyclin activation of* $p34^{cdc2}$, **Cell 63**, pp 1013-1034, 1990.

[6] M.A. Felix, J.C. Labbe, M. Doree, T.Hunt, and E. Karsenti, *Triggering of cyclin degradation in interphase extracts of amphibian eggs by cdc2 kinase*, **Nature 346**, pp 379-382, 1990.

[7] A.W. Murray and M.W. Kirschner, *Cyclin synthesis drives the early embryonic cell cycle*, **Nature 339**, pp 275-280, 1989.

[8] M. Dasso and J.W. Newport, *Completion of DNA replication is monitored by a feedback system that controls the initiation of mitosis in vitro: studies in Xenopus*, **Cell 61**, pp 811-823, 1990.

[9] William E. Boyce and Richard C. DiPrima, **Elementary Differential Equations and Boundary Value Problems**, John Wiley and Sons, New York, 1977.

[10] Ali Nayfeh, **Nonlinear Dynamical Systems and Chaos**, Prentice Hall, Englewood Cliffs, 1983.

[11] Richard K. Miller and Anthony N. Michel, **Ordinary Differential Equations**, Academic Press, New York, 1982.

[12] John Guckenheimer and Philip Holmes, **Nonlinear Oscillations, Dynamical Systems, and Bifurcations of Vector Fields**, Springer-Verlag, New York, 1983.

[13] V.I. Arnold, **Geometrical Methods in the Theory of Ordinary Differential Equations**, Springer Verlag, New York, 1988.

[14] S. Wiggins, **Introduction to Applied Nonlinear Dynamical Systems and Chaos**, Springer Verlag, New York, 1990.

[15] Yuri A. Kuznetsov, **Elements of Applied Bifurcation Theory**, Spinger Verlag, New York, 1995.

[16] Steven H. Strogatz, **Nonlinear Dynamics and Chaos**, Addison-Wesley Publishing Company, Reading Massachusetts, 1994.

[17] John Guckenheimer, *Multiple bifurcation problems for chemical reaction*, **Physica 20D**, pp 1-20, 1986.

[18] Stephen Schecter, *The Saddle Node Separatrix Loop*, **SIAM Journal of Math Analysis 18**, pp 1142-1156, 1987.

[19] Bela Novak and John J. Tyson, *Modeling the Cell Division Cycle: M-phase Trigger, Oscillations, and Size Control*, **Journal of Theoretical Biology, 165**, pp 101-134, 1993.

[20] John Guckenheimer, *Bifurcation of the Hodgkin and Huxley Equations: A New Twist*, **Bulletin of Mathematical Biology Vol. 55 No. 5**, pp 937-952, 1993.

[21] E.J. Doedel and X.J. Wang *AUTO94 : Software for continuation and bifurcation problems in ordinary differential equations*, **Technical report**, Center for Research on Parallel Computing, California Institute of Technology, Pasadena, CA 91125. CRPC-95-2.

[22] A. Back, J. Guckenheimer, M. Myers, F. Wicklin, and P.Worfolk, *dstool: Computer Assisted Exploration of Dynamical Systems*, **Notices of the American Mathematical Society Vol.39**, pp 303-309, 1992.

[23] A. Champneys, Y. Kuznetsov, and B. Sandstede, *A numerical toolbox for homclinic bifurcation analysis*, To appear.

Vita

I was born on August 3, 1968. I grew up on a farm in the finger lakes region of upstate New York where I learned to appreciate the outdoors, life, and the complexity of living things. I graduated from Bob Jones University in 1990 with a B.S. in Mathematics. After graduating I came to Viginia Tech. Since 1991 I have been employed as either a research or teaching assistant. Courses that I have taught include Calculus with *Mathematica* and Differential Equations. I recieved my M.S. in Mathematics in 1993 and begun work with Dr. John J. Tyson the summer of 1994.